Petrographic observations and evaporate mound analysis of quartz-hosted fluid inclusions hosted by granitoid samples from the South Mountain Batholith, Nova Scotia: An exploration tool for vectoring towards mineralised areas in intrusive rocks

Fergus Tweedale[1], Jacob J. Hanley[1], Dan J. Kontak[2] and Neil Rogers[3]

1. Department of Geology, Saint Mary's University, 923 Robie St., Halifax, Nova Scotia
2. Department of Earth Sciences, Laurentian University, 935 Ramsey Lake Rd., Sudbury, Ontario
3. Geological Survey of Canada, 601 Booth St., Ottawa, Ontario

Abstract: The ca. 380 Ma South Mountain Batholith (SMB) of Nova Scotia is a large (ca. 7,300 km^2), mesozonal granitoid intrusion that consists of 13 coalesced plutons of granodiorite to leucomonzogranitic composition which host a variety of mineralised zones (e.g., Sn-Zn-Cu-Ag, Mo, Mn-Fe-P, U, Cu-Ag). Given the hydrothermal nature of this mineralisation, it is expected that a fingerprint of the mineralizing fluids might be manifested both petrographically and by the chemistry of secondary, quartz-hosted fluid inclusions in the granites on a scale equal to or larger than the mineralised centres. In order to assess the potential of using the petrographic and chemical fingerprints as vector for exploration, a study integrating both these methods was investigated. The protocol involved in the study included the following: (1) completing a detailed petrographic study of hundreds of archived thin section samples that focused on the extent and degree of alteration that reflect fluid-rock interaction. The indices included: (i) type and abundance of perthite, (ii) chloritic alteration of biotite, (iii) plagioclase alteration, (iv) amount of secondary white mica, and (v) abundance of secondary fluid inclusions in quartz; and (2) determining the fluid chemistry of quartz-hosted fluid inclusions in samples (n = 66) collected from the SMB. For this study, a detailed protocol was developed to address specific analytical considerations, including decrepitation temperature, oven versus stage heating, EDS calibration, EDS acquisition time, representative sampling and raster versus point mode of analysis. Thus, in this study, quartz chips were heated to 500ºC and a maximum of 16 mounds per sample were analysed (60 seconds) in raster mode, the latter to circumvent chemical variation related to elemental fractionation during mound formation. To date, the results indicate that the fluids from Phase 1 samples are dominated by a Na-F-Cl-Ca fluid. In contrast, fluids from Phase 2 samples are dominated by two fluid inclusion populations: a Na-K fluid and a F-Na-Cl-Ca fluid.

Introduction

Fluid inclusions are microscopic (i.e., <50 μm) samples of paleofluids that circulated at some time during the hydrothermal history of the host mineral, and in mineralised areas, may be associated with hydrothermal ore deposits. The composition of fluid inclusions therefore, provides chemical data that is relevant to the modelling of ore deposits and the design of exploration strategies (Roedder and Bodnar, 1997). A problem associated with categorizing large granitoid intrusions that host ore deposits is the simultaneous management of environmental and economic costs and the collection of data that is representative of the entire system. To address this problem, we propose the development and testing of a cost-effective and time-efficient exploration technique that is a useful for regional-scale characterization of fluid-rock interaction, called evaporate mound analysis. The technique involves the controlled decrepitation (i.e., bursting) of quartz-hosted fluid inclusions and chemical analysis of the resultant evaporate mounds with an electron probe equipped with a high resolution imaging system. The ca. 7,300 km^2, mineralised South Mountain Batholith (SMB), Nova Scotia, is largest granitoid intrusion in the northern Appalachians (Fig. 1). The SMB is also one of the most intensively studied peraluminous granitoid complexes in the world (Chatterjee and Clarke, 1985), and the abundance of accessible outcrop, as well as the preservation of archived thin section and slab collections housed by the Nova Scotia Department of Natural Resources, make the SMB an ideal testing ground for evaporate mound analysis. Additionally, SMB quartz hosts abundant liquid-rich secondary fluid inclusions. This paper provides a framework describing the methodology behind SEM-EDS analysis, including step-by-step details regarding sample preparation, artificial decrepitation procedures, SEM-EDS analytical protocols, application of calibration standards, EDS data-reduction considerations, and data-display options. The methodology was refined through examination of a suite of granitoid samples collected from the contiguous and fertile SMB. This research evaluates fluid chemistry in an effort to better characterize a fertile metal system by providing a regional-scale assessment that can guide future studies. The results of this work will help determine if evaporate mound analysis, when combined with petrographic work, is a viable exploration tool. This Targeted Geoscience Initiative 4 (TGI 4) funded work is a

Corresponding author: Fergus Tweedale (fergus.tweedale@gmail.com)

Tweedale, F., Hanley, J.J., Kontak, D.J., and Rogers, N., 2015. Petrographic observations and evaporate mound analysis of quartz-hosted fluid inclusions hosted by granitoid samples from the South Mountain Batholith, Nova Scotia: An exploration tool for vectoring towards mineralised areas in intrusive rocks; *in* TGI 4 – Intrusion Related Mineralisation Project: New Vectors to Buried Porphyry-Style Mineralisation, (ed.) N. Rogers; Geological Survey of Canada, Open File 7843, p. 79-99.

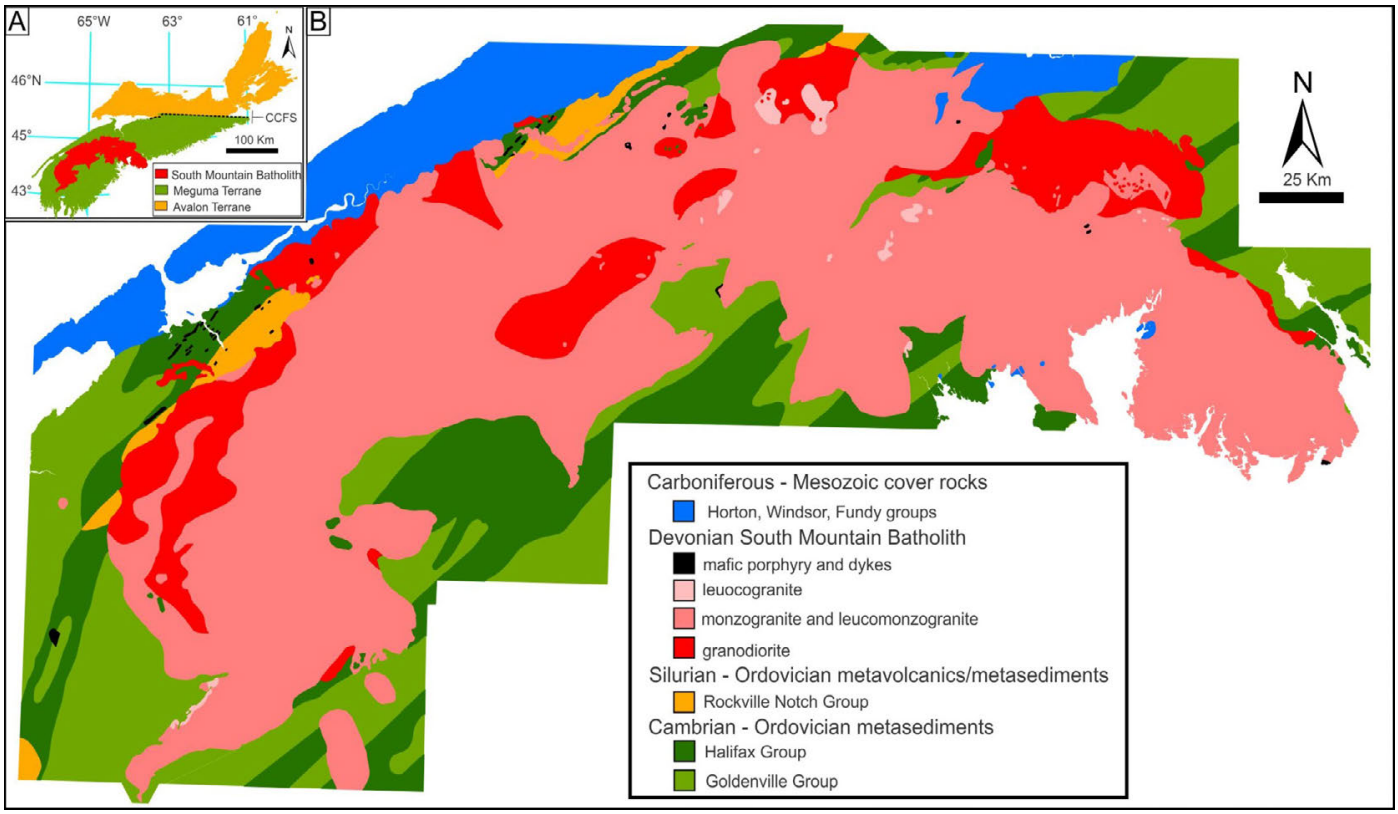

Figure 1 – Geological map of study area. (A) Index map showing simplified geology of Nova Scotia, showing the two terrane units separated by the Cobequid Chedbucto Fault System (CCFS). The South Mountain Batholith (SMB) intrudes the Meguma terrane, the most outboard terrane of the Appalachian Orogen. (B) Geological map of the SMB. Map boundaries from the Nova Scotia Department of Natural Resources.

test case and is the first of its kind conducted on a batholithic scale, with the resulting methodological protocols being readily exportable for mineral fertility assessment of other areas

Relevance of analytical technique

Fluid-filled cavities in minerals, called fluid inclusions, are trapped samples of the ambient fluid that circulated during mineral growth (i.e., primary fluid inclusions) or during post-crystallisation alteration (i.e., secondary fluid inclusions; Timofeeff et al., 2000; Ménez et al., 2002). Aqueous fluid inclusions therefore provide an opportunity to directly analyse the chemical composition and evolution of fluids involved with magmatic-hydrothermal ore deposition. Microthermometry is the most frequently used technique to evaluate fluid inclusion salinity, but results reported in equivalent wt% NaCl units can provide only qualitative detail, and cannot account for undetermined cation and anion solutes. Metastability affecting phase change behaviour also invites caution (Kontak, 2004). Other conventional methods used for solute analysis of fluid inclusions include crush-leach techniques to extract the fluid followed by LA-ICP-MS compositional analysis. However, the results obtained from crush-leach analysis reflects multiple generations of fluids (Chi et al., 2003), and the electronegativity of fluorine, a potential ore metal complexation ligand in magmatic-hydrothermal fluids (McPhie et al., 2011; Thomas et al., 2006; Wilkinson, 2001; Muecke and Clarke, 1981) precludes application of standard LA-ICP-MS analysis (Bu et al., 2003). Scanning electron microscopy/energy dispersive X-ray spectroscopy (SEM-EDS) evaporate mound analysis, is a cost effective alternative method to obtain in-situ solute analysis of fluid inclusions (Kontak, 2004).

Previous studies

By employing relatively low-cost equipment and time-efficient methodology, evaporate mound analysis is an effective approach for characterizing fluid inclusion solute chemistry in a variety of magmatic-hydrothermal settings. Previous work indicates that SEM-based methods produce semi-quantitative chemical analyses of fluid inclusions hosted in minerals in a variety of geologic settings, including volcanogenic massive sulphide deposits (Zaw et al., 2003), Mississippi Valley-type deposits (Haynes and Kesler, 1987; Savard and Chi, 1998), carbonitite-hosted deposits (Samson et al., 1995), metamorphosed strata-bound copper depsoits (Heinrich and Cousens, 1989), and granite-hosted mineral deposits (Chryssoulis and Wilkinson, 1983; Kontak et al., 1999; Carruzzo et al., 2000; Kontak, 2004).

Of the numerous techniques used to analyse fluid inclusion solute chemistry (see Chi et al. (2003) for a summary review), only crush-leach ion chromatography, laser ablation inductively coupled plasma mass spectrometry (LA-ICP-MS) and SEM-EDS evaporate mound analysis are comparable in terms of sensitivity to solute cations and anions. Many other techniques used in fluid inclusion research are analytically challenging (i.e., time-inefficient) and/or provide data expressed in relative units (i.e., wt% NaCl). For example, secondary ion mass spectrometry (SIMS) analysis can, in principle, provide detection for all elements (Diamond et al., 1990), but the analytical complexity (Ménez et al, 2002) and the prohibitive cost (Gleeson, 2003) of

this technique impair its practicality as an exploration tool. Other microbeam-based techniques including synchrotron X-ray fluorescence (SXRF), proton-induced X-ray emission (PIXE) and proton-induced gamma emission (PIGE) require time-consuming sample preparation and long analytical times (Ménez et al., 2002; Anderson and Mayanovic, 2003). Additionally, PIXE and PIGE mostly yield only cation data (Gleeson, 2003), and solute concentration measurements using SXRF demand tedious measurement of the microscopic volume of the inclusions (Frantz et al., 1988).

It should also be emphasized that SEM-EDS analysis has advantages over LA-ICP-MS and bulk crush-leach techniques. Crush-leach analyses integrate a protracted hydrothermal history (i.e., solute compositions of fluid inclusion assemblages and single inclusions are not resolvable). Although costly in terms of time and equipment, LA-ICP-MS is a highly sensitive technique, but electronegativity issues regarding some halogens (i.e., metal ligands) makes some (e.g., F) elements undetectable (e.g., Bu et al., 2003).

Geological setting of the South Mountain Batholith

The mineralised SMB, located within the Meguma Zone of the Appalachian Orogen, is a post-tectonic granitoid complex of Devonian age (ca. 380 Ma; Clarke and Halliday, 1980; Reynolds et al., 1981). The batholith intrudes the regionally metamorphosed (greenschist-amphibolite facies) Cambrian to Ordovician Meguma Supergroup (MS) and the overlying Ordovician to Silurian Rockville Notch Group (RNG). The MS comprises a thick (>10 km) sequence of folded metasedimentary strata that includes the lower, sandstone-dominated Goldenville Group and the overlying siltstone-dominated Halifax Group. The SMB contact with the RNG trends NE-SW and is overlain in some areas by Carboniferous cover rocks. The RNG comprises mixed volcanic, volcanoclastic and metasedimentary rocks, and the overlying cover rocks include the coarse-clastic terrestrial sedimentary rocks, evaporites sequences and volcanoclastic rocks of the Mississippian Horton, and the Triassic Windsor and Fundy groups, respectively (Fig 1). In general terms, the SMB is a composite intrusion of granodiorites, monzogranites, leucomonzogranites and leucogranites, locally cut by metre-scale pegmatite dykes and aplite sheets. Outcrop-scale structures within the SMB (Fig. 2) provide clear evidence that late-stage fluid flow is part of the hydrothermal history of the batholith.

Based on field relationships and compositional variations identified during research conducted by the NSDNR (MacDonald, 2001) SMB rock units are grouped into 13 plutons, which include five Stage 1 plutons and eight Stage 2 plutons (Fig. 3). The earlier Stage 1 plutons mainly consist of biotite granodiorite and biotite monzogranite. Stage 2 plutons intrude Stage 1 plutons. Stage 2 plutons mainly consist of two-mica monzogranite, fine- and coarse-grained leucomonzogranite and muscovite leucogranite. Internal contacts can be either intrusive or gradational (MacDonald, 2001).

Known Mineralisation within the South Mountain Batholith

The SMB is host to the past-producing East Kemptville (Sn-Zn-Cu-Ag) and New Ross Manganese (Mn-Fe-P) mines, the Millet Brook (U-Cu-Ag) deposit, as well as numerous other polymetallic prospects and occurrences (Fig. 4).

Four main deposit types occur within the SMB: greisen, vein, breccia and pegmatite. Although associated with the SMB, peribatho-

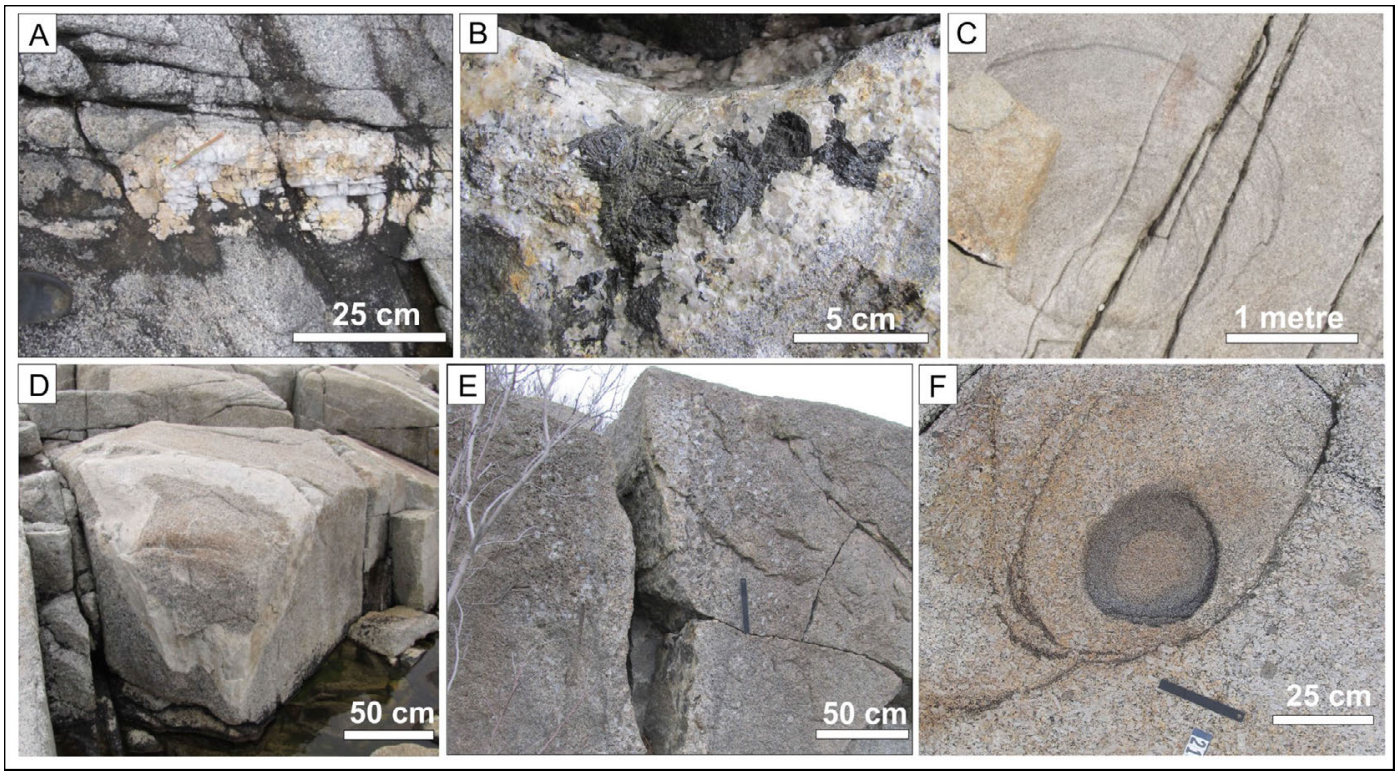

Figure 2 – Macroscopic-scale evidence of hydrothermal fluid flow in the SMB. (A) Miarolitic cavity near Aspotogan Point in Lunenburg County. (B) Tourmaline clot in the Halifax Pluton. (C) Ring schlieren at Pennant Point, Halifax County. (D) Aplite sheet at Peggy's Cove. (E) Breccia pipe in highway outcrop near Halifax. (F) Biotite schlieren near municipality of Prospect.

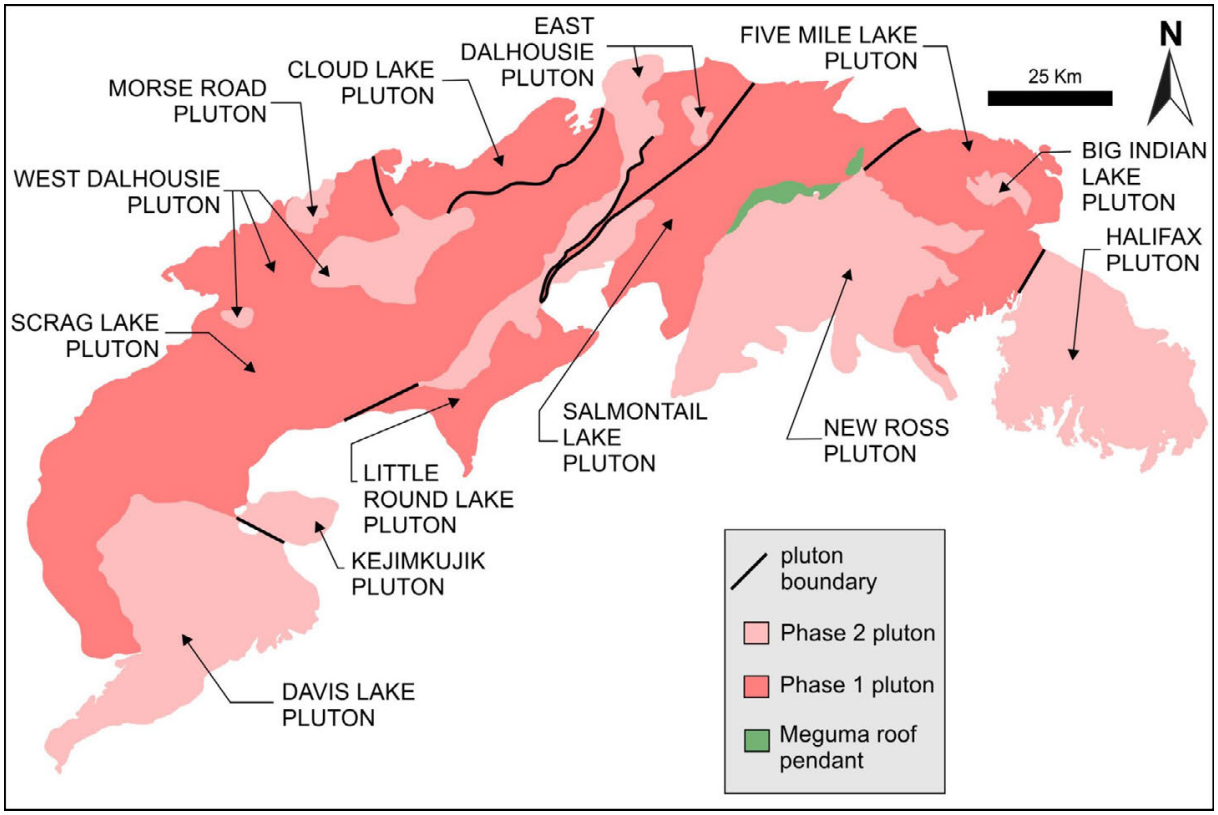

Figure 3 –Map of South Mountain Batholith pluton boundaries Phase 1 plutons are generally biotite-granodiorites and biotite monzogranites. Later Phase 2 plutons are generally 2 mica monzogranites, leucomonzogranites and leucogranites (MacDonald, 2001).

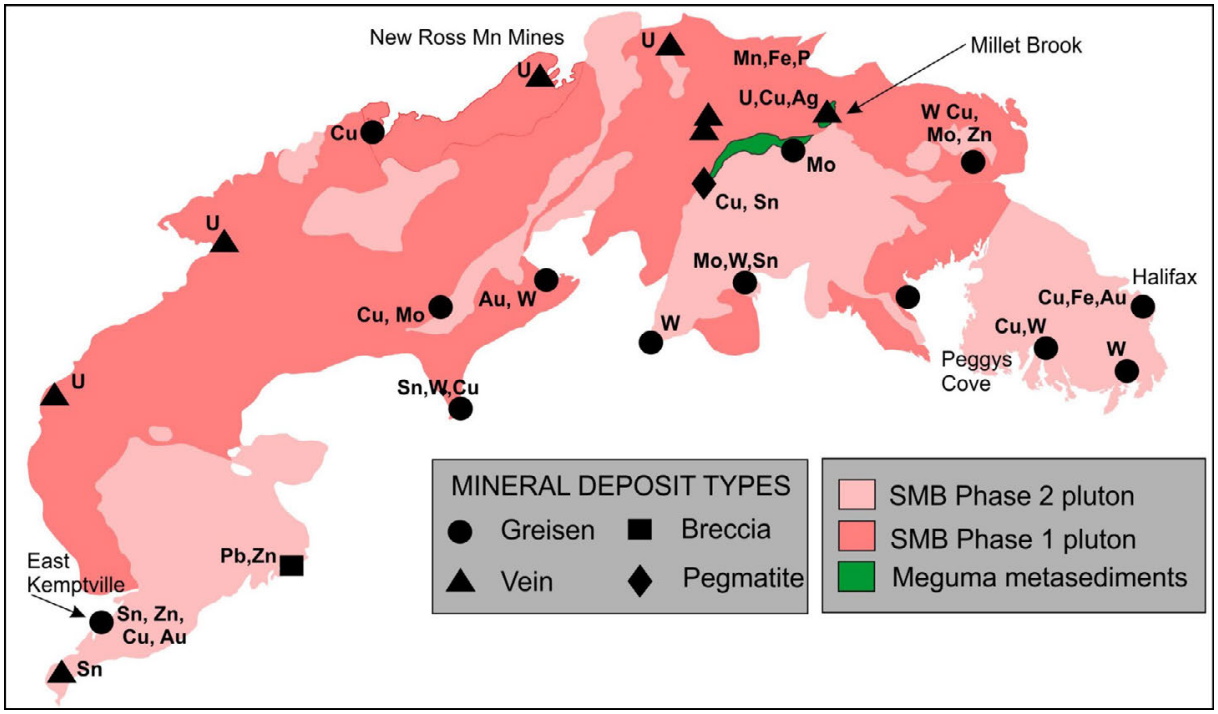

Figure 4 – Locations of major known mineral deposits hosted by the South Mountain Batholith (modified from MacDonald, 2001). The great diversity in style (e.g., greisen, vein, breccia and pegmatite) and in metal assemblages (e.g., Sn-Zn-Cu-Ag, Mo, Mn-Fe-P, U, Cu-Ag) of SMB mineralised centres are the result of post-crystallisation hydrothermal processes.

lithic (endogranitic) deposits (MacDonald et al., 2002; Kontak, 1990) occurring near contact areas with the Meguma rocks are not discussed. Brief details of each of the SMB deposit types are discussed below.

Greisen deposits (Sn-W-Mo-As-Cu-Pb-Zn-F-Au-Ag)

Greisen occurs in SMB rocks that range in composition from the least-evolved granodioritic phases (e.g., Sandwich Point prospect) to the most evolved muscovite-leucocratic phases (e.g., East Kemptville deposit), and tends to occur primarily in the Stage 2 plutons. Typically SMB greisens are spatially associated with major structural features. However, the underlying genetic relationship between major structural features and ore deposition associated with greisen occurrence remains unclear. Whereas the SMB greisens are distributed throughout the batholith, the largest greisen-style mineral occurrences are typically proximal to shallow-dipping contact zones between the granite and Meguma metasedimentary rocks. The past-producing East Kemptville Sn-Zn-Cu-Ag occurrence is the largest known economic SMB-hosted deposit, and it occurs at the SMB-Meguma contact within the regional East Dalhousie East Kemptville Shear Zone (EKEDSZ). Greisen associated with the Long Lake Mo-W-Cu prospect west of the municipality of Chester Grant in Lunenburg County, and the W-Sn-Mo-Cu-Zn-Ag-Au prospect at Westfield in Queen's County are proximal to granite-metasediment contacts that are not associated with major faults (O'Reilly, 2011, 2013; Cormier, 1988). However, greisen mineralisation is also associated with vein-type deposits, including the Sandwich point prospect that occurs adjacent to vein mineralisation (Au-Bi-Sb-Cu-Zn) that cuts SMB monzogranite near the Meguma – SMB contact (Kontak and Kyser, 2011). From this, it appears evident that greisen form preferentially near SMB-metasedimentary contact zones that are proximal to fault zones.

Of particular relevance for fluid inclusion studies, past research suggests that SMB greisens are intimately associated with hydrothermal fluids. For example, Clarke et al. (1993) interpret the results of field, petrologic and geochemical studies to suggest that hydrothermal alteration of fine-grained leucomonzogranites produced the muscovite -leucogranites greisens and associated mineralised centres of the Long Lake prospect. From an evaluation of compositional and mineralogical changes in a zoned greisen, Halter et al. (1996) substantiated the role of fluid–rock interaction in forming the East Kemptville deposit. Elevated concentrations of Bi and Au are a unique chemical signature of the Inglisville greisens, which MacDonald and O'Reilly (1989) associate with the circulation of hydrothermal fluids through the Meguma metasediments proximal to their contact with the SMB. Understanding the solute chemistry of fluid inclusions may provide information that is helpful in resolving the development of these deposits.

Vein deposits (U-Cu-Mn-P-F-Ag)

Whereas greisen deposits tend to occur in Stage 2 plutons, vein deposits of economic interest occur dominantly in Stage 1 plutons. Most of the past-producing vein deposits are within the interior of the batholith, including the New Ross Manganese Mines that are hosted by the Stage 1 Salmontail Lake Pluton. In contract to the greisen deposits, U and Mn are economically significant commodities of vein deposit mineralisation (MacDonald, 2001).

The Millet Brook U-Cu-Ag deposit occurs near a Meguma roof pendant in Lunenburg County. Pitchblende is the dominant ore mineral, but minor chalcopyrite, bornite, covellite, chalcocite, proustite, galena, sphalerite and wolframite also occur (MacDonald, 2001). The en-echelon distribution of the mineralised veins (i.e., ore zones) suggests structural influence. Hematization (i.e., turbid feldspar) and chloritization of biotite are closely associated with some ore-zones,

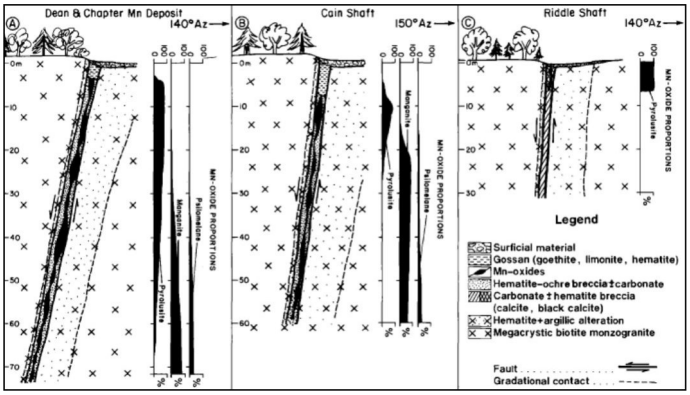

Figure 5 – Cross section schematic of the New Ross Manganese Mines (copied from O'Reilly, 1992). Ore minerals at the Dean & Chapter and Cain & Riddle mines include manganite (MnO(OH), Pyrolusite (MnO_2), Psilomelane ($Ba,H_2O)_2$ Mn_5O_{10}, fluoroapatite $Ca_5(PO_4)_3F$ and manjiroite $(Na,K)(Mn^{4+},Mn^{2+})_8O_{16}.n(H_2O)$.

suggesting that fluid–rock interaction played a role in ore deposition at Millet Brook (MacDonald, 2001).

Similarly, the most pervasive alteration associated with the economic mineralisation at the New Ross Manganese Mines (Mn-Fe-P) is hematization, but desilification, albitization and sericitization are also observed (O'Reilly, 1992). Located near the municipality of New Ross, in Lunenburg County, the New Ross Manganese Mines include the past-producing Cain and Riddle Mine and the Dean and Chapter Mine. At these mine sites, ore bodies occur along steeply dipping faults that are interpreted as being localised along pre-existing structural features (Fig. 5). Several types of hydrothermal alteration have been observed. Hematization and sericitization are well developed in the ore veins, and the co-precipitation of fluoroapatite and Mn-oxides suggests the presence of a phosphate-bearing fluid at low temperature (O'Reilly, 1992). Moreover, and adding pertinence to this fluid inclusion study, O'Reilly (1992) suggested that the alteration sequence at the New Ross Mines could be part of an evolving, and potentially regional, hydrothermal system, which suggests a potential for as yet undiscovered deposits of granophile mineralisation (Smith and Turek, 1976).

Breccia deposits (Pb-Zn-Ba-Au-Ag)

Known SMB breccia deposits (Pb, Zn, Ba, Au, Ag) are spatially restricted to the area proximal to the Tobeatic fault zone (TFZ) in the southwest portion of the batholith, where exploration efforts are hindered by poor outcrop control and metre-scale overburden (Giles, 1985). Extending approximately 8 km in length, and averaging 100 m in width (Giles, 1985), the TFZ coincides with the southern extent of the larger Tobeatic Lake Shear Zone (Horne et al., 1992). Disseminated combinations of galena, sphalerite, barite, chalcopyrite, arsenopyrite and pyrite have been observed in brecciated boulders (MacDonald, 2001). Based on anomalous high concentrations of Zn, Pb, Sn, W and Au in regional till samples, Corey and Horne (1989) suggest the area to be a prime base metal and precious metal exploration target.

Pegmatite deposits (Sn-W-U-Cu-Zn-Ag)

The New Ross Pluton hosts all the reported pegmatite mineral deposits within the SMB, but unmineralised pegmatites are associated

with the East Kemptville deposit, the Gaspereau Lake U-P-F prospect and the Long Lake deposit (MacDonald, 2001, and references therein). Coarse-grained leucomonzogranites and leucogranites host the known pegmatite deposits. Although previous exploration did not indicate a significant resource potential for SMB pegmatite deposits, two known prospects draw particular interest as they have not been subjected to detailed exploration, and thus have unknown economic potential. Firstly, the Keddy Mo-Ta-Nb prospect, hosted in the Keddy-Reeves muscovite-topaz leucogranite, occurs near the boundary between the Stage 1 Salmontail Lake Pluton and the Stage 2 New Ross Pluton. Secondly, the spodumene- and tourmaline-bearing pegmatites of the Brazil Lake prospect are considered to have economic potential for Be and Li (Corey, 1994).

Methodology

Sampling strategy

The objective for this regional-scale research is to obtain a sample set that represents the entire SMB study area. We use a grid system to systematically divide the study area into a number of sampling targets. A 10 x 10 km^2 grid was superimposed on the SMB map pattern (Fig. 6) and an ideal sample set would include one sample from each grid square. However, samples in some grid locations are inaccessible due to poor outcrop exposure due to glacial overburden (e.g., the Scrag Lake Pluton), therefore, grid sampling in principal provides only a general guideline. In some cases, where several rock types occur in a given grid square, a sample of each rock type was collected.

Evaporate Mound Analysis

Indices of Alteration

Characterizing the extent and degree of fluid-rock interaction and locating quartz grains that host abundant fluid inclusions are the objectives of the petrographic work which must be completed prior to evaporate mound analysis. Following identification of alteration assemblages that occur in the study area, the degree or extent of the alteration is qualitatively assessed. Assessment is measured on a nominal scale where a value of '1' represents the lowest degree or extent of alteration and '10' represents an extreme or high degree of alteration. For the SMB appropriate indices include (i) chloritization of biotite, (ii) abundance and type of perthite, (iii) sericitization and (iv) saussuritization (Fig. 7), (v) the abundance of white mica (Fig. 8), and the abundance of fluid inclusions hosted by quartz (Fig. 9).

Preparation of fluid inclusion wafers

The preparation of double polished thick sections requires the cutting and grinding of slab samples into ca. 150 µm fluid inclusion wafers that are bonded to glass slides for petrographic examination. Sections (i.e., chips) that include target mineral grains are cut from the wafer using a fine circle blade appropriate for cutting small centimetre -scale chips. Following the experience from cutting hundreds of sections, we recommend a minimum section size of 1 cm^2 for ease of handling during further processing (Fig. 10).

Mound generation and decrepitation temperature

Published results of other evaporate mound research report a range of decrepitation temperatures (Table 1). However, there are no published reports that assess the effect of decrepitation temperature on mound generation, mound size, and mound composition. To address these issues, we selected a small subset of samples (n = 3) and prepared three chips from each sample for experimental heating. Three temperatures, 325°C, 400°C and 500°C (one grain/sample for each temperature) were selected. In addition we compare results from mounds generated by heating in an oven and a heating-freezing stage. The oven heating rate was 1°C/minute and the stage heating rate was 20°C/minute. The oven is Thermacraft clamshell furnace and the stage

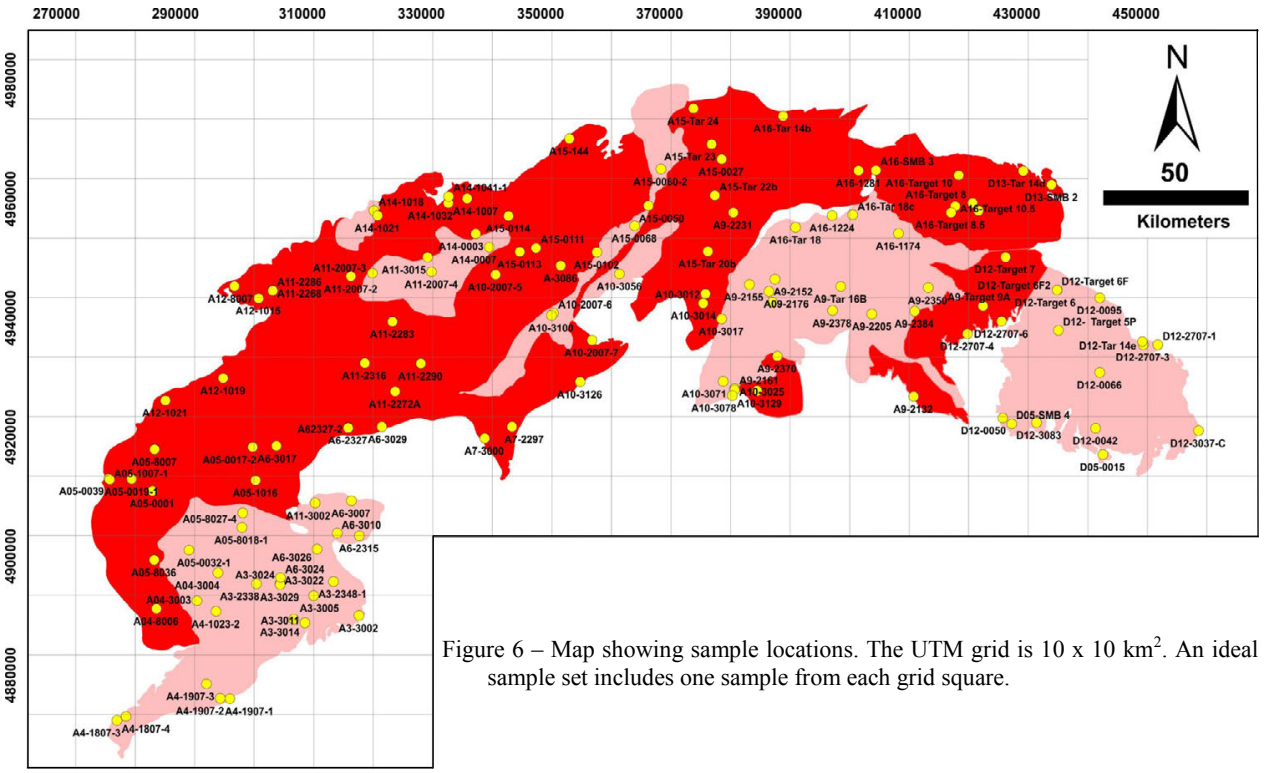

Figure 6 – Map showing sample locations. The UTM grid is 10 x 10 km^2. An ideal sample set includes one sample from each grid square.

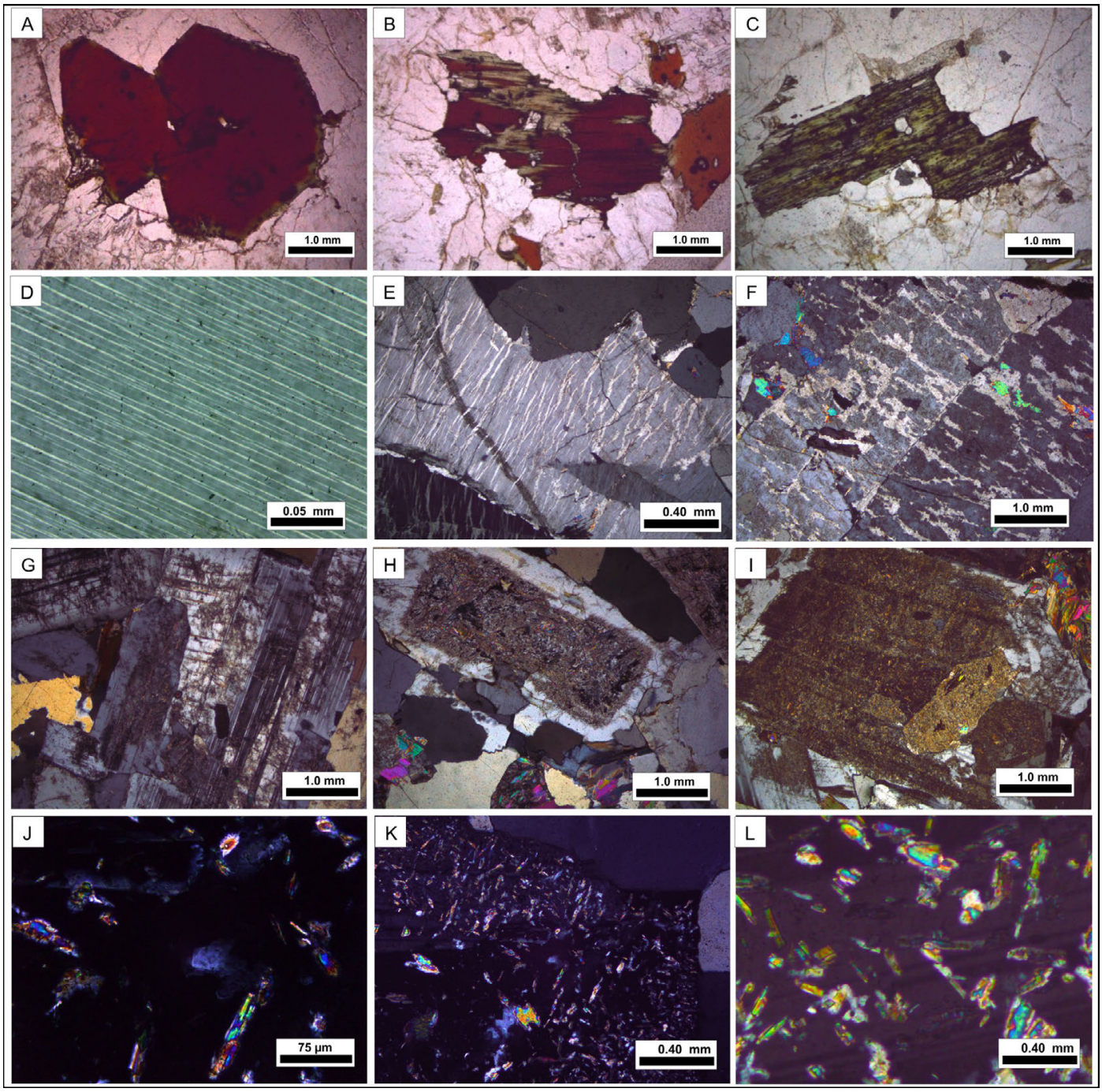

Figure 7 – Photomicrograph images of alteration indices used to determine the degree of fluid–rock interaction in SMB granitoid samples. (A-C) Chloritization of biotite. (D-F) Perthite. (G-I) Sericite. (J-L) Saussuritization. In all four indices, fluid–rock interaction increases from a minimum in the left photomicrograph to a maximum in the right photomicrograph.

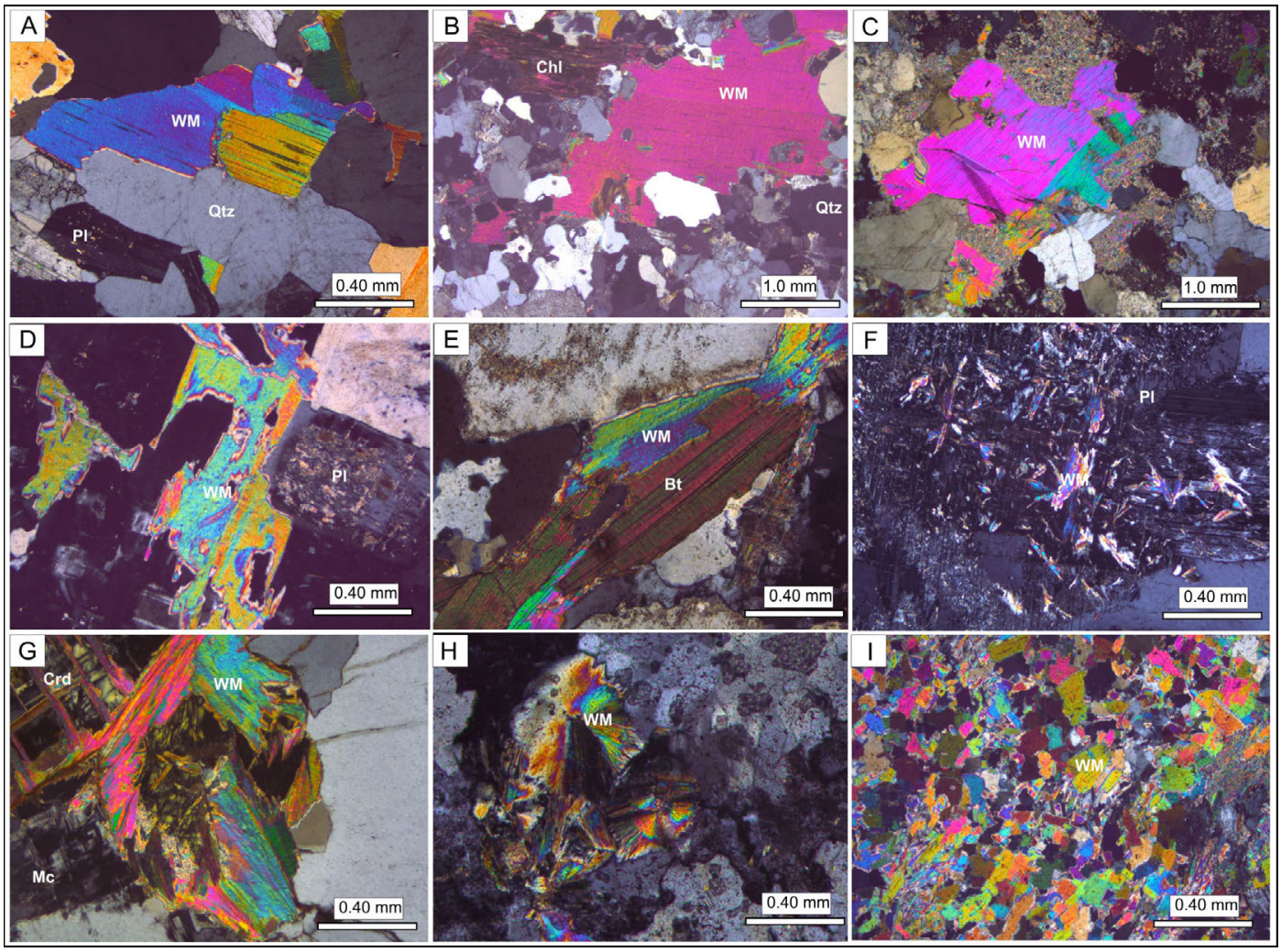

Figure 8 – Photomicrographs of thin sections displaying white mica varieties in SMB granitoid samples. Mineral abbreviations: Crd: cordierite; Mc: microcline; Pl: plagioclase; Qtz: quartz; WM: white mica. (A) Sample LU87-4: coarse-grained, euhedral and equant white mica grain displaying sharp crystal boundaries in equigranular leucomonzogranite. (B) Sample D12-0124-3: coarse-grained, subhedral white mica in quartz matix showing extensive development of sutured grain boundaries and allotriomorphic texture. Biotite grain adjacent to white mica is extensively chloritized. (C) Sample A09-2229: prominent kink in crystal face (001) of coarse-grained white mica that shows extensive sericite alteration along embayed grain boundary. (D) Sample A09-2211-2: white mica overgrowth on alkali feldspar grain. (E) Sample D05-3105: white mica replacing an earlier biotite phase. Note both mica phases share common optical orientation. (F) Sample BILP-3: medium-grained white mica clusters on an earlier plagioclase phase. (G) Sample D05-3105: white mica replacement of cordierite adjacent to microcline. (H) Sample D12-0122-2: clusters of white mica rosettes in altered granite from the Halifax pluton. (I) Sample A15-0008-4: white mica greisens.

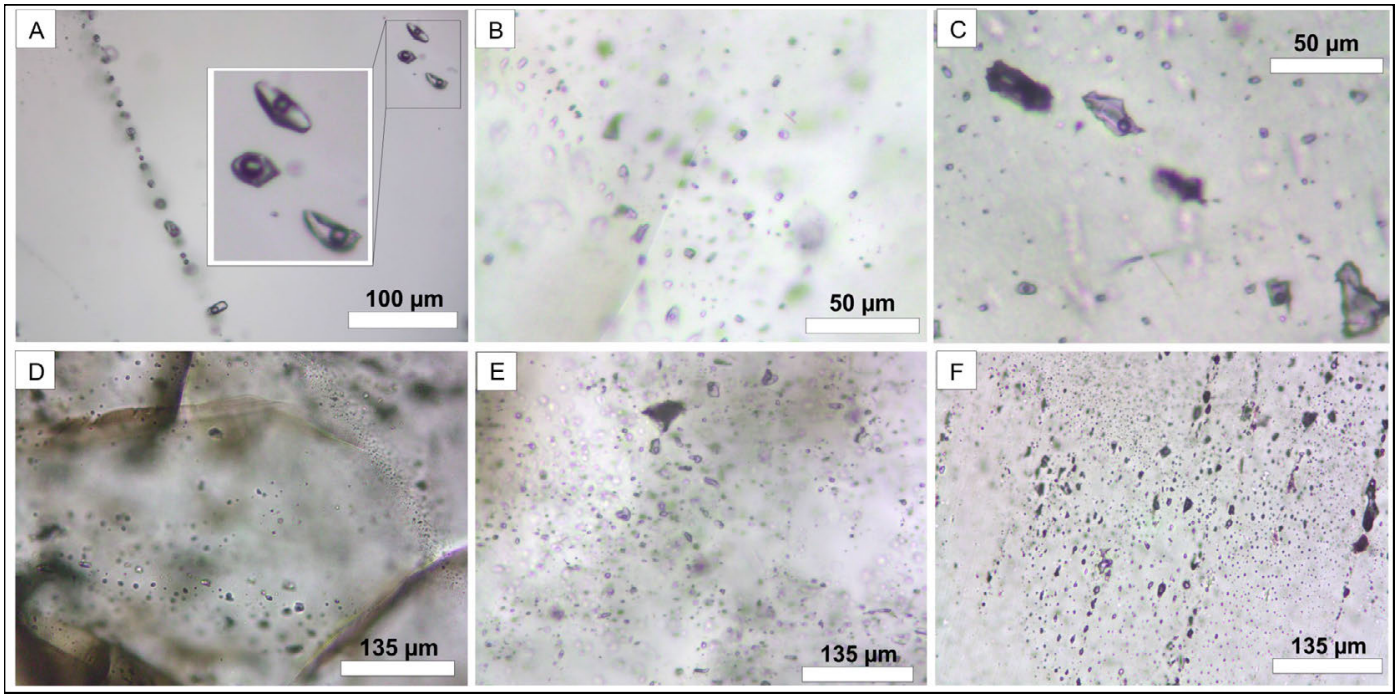

Figure 9 – Photomicrographs of thin sections displaying secondary fluid inclusions in annealed quartz in SMB granitoid samples. (A) Sample A09-0045: two-phase LV-type fluid inclusions forming linear arrays and isolated fluid inclusion assemblages in quartz. (B) Sample A03-3024-2: Inundation of variably-sized two-phase (LV) and monophase (L) fluid inclusions. (C) Sample A04-3004-2: large (15 µm), irregularly-shaped fluid inclusions with common long-axis orientation. (D) Sample A09-3024: fluid inclusion arrays showing orientations that do not coincide with grain boundary orientations. (E) Sample A09-2378: fluid inclusion inundation hosted by quartz in a monzogranite sample from the New Ross pluton. (F) Sample A16-1400: 2-phase (L-V) and monophase (V) fluid inclusions. Note large range in fluid inclusion size.

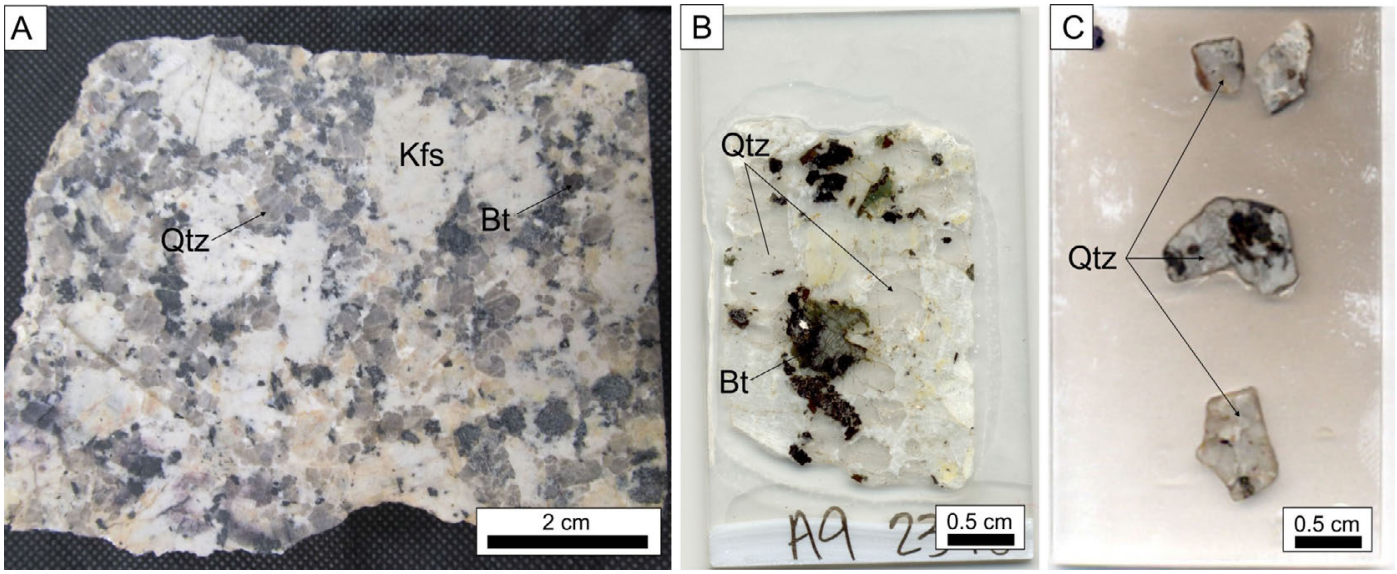

Figure 10 – Preparation of samples for SEM-EDS analysis. (A) A slab sample for each grid square covering the study area is collected. (B) Fluid inclusion wafers are prepared for petrographic evaluation and identifying of targeted fluid inclusions. (C) Chips containing fluid inclusion host mineral, quartz, are cut from wafer and immediately carbon coated (10 – 20 µm veneer). Carbon mitigates charge build-up during SEM-EDS analysis.

Table 1 – Decrepitation temperature ranges used in other evaporate mound research.

Host rock	Host mineral	Dominant fluid inclusion type	Decrepitaion temp. range(°C)	Reference
n/a	*synthetic quartz*	*2-phase L-V*	*360 - 420*	*Haynes et al., 1988*
altered granite, pegmatite, greisen, veins	*quartz*	*L-V, L-V-H, L-V-H-Sylvite*	*350 - 500*	*Kontak 2004*
granitoid	*quartz*	*L-rich, V-rich, L-V, L-V±S, L-V-H*	*400 - 420*	*Carruzzo et al., 2000*
carbonitite	*apatite, calcite*	*L-V, L-V-H*	*400 - 500*	*Samson et al., 1995*
carbonate	*calcite, dolomite, sphalerite*	*not given*	*420*	*Savard and Chi, 1998*
breccia/quartz syenite	*fluorite, quartz, bastnaesite, barite*	*L-V-S, L-V, A-C*	*400*	*Williams-Jones et al., 2000*
quartz-kaolinite breccia	*quartz*	*L-V*	*450 - 600*	*Kontak and Kyser, 2011*
veins hosted in granite	*quartz*	*V-rich, L-rich, L-S, V-S*	*up to 570*	*Chryssoulis and Wilkinson, 1983*
brecciated carbonate	*sphalerite and dolomite*	*not specified*	*325 - 350*	*Haynes and Kesler, 1987*
rhyolite/sedimentary	*quartz*	*L-V*	*350-400*	*Zaw et al., 2003*
vein infill	*quartz, sphalerite*	*L(H_2O-CO_2-CH_4)-S*	*500*	*Walsh et al., 1988*
metasedimentary	*quartz*	*L-V*	*300 - 350*	*Heinrich and Cousens, 1989*

Abbreviations for fluid inclusion types: aqueous-carbonic, A-C; halite, H; liquid, L; solid, S; vapour, V.

is a Linkham MDS600 heating –freezing stage mounted on a standard petrographic microscope stage. Following decrepitation, all samples are immediately carbon coated and stored in a desiccation chamber until taken to the SEM.

SEM-EDS operating conditions and acquisition time

The LEO 1450VP SEM used in this study was operated with a tungsten filament saturated at 3.2-3.3 A, an accelerating voltage of 25 keV and a working distance range of 17 to 21 mm. The SEM imaging system is equipped with an Oxford Instrument INCA X-max 80 mm^2 silicon drift detector (SDD) EDS analyser linked to a desktop computer (INCA software). In this experimental study, point mode was used to analyse small (i.e., < 5 µm diameters) mounds, and raster mode used to analyse large, irregularly shaped mounds. Results obtained using point and raster modes are reported here. A 60 second acquisition time was used for all analyses. However, in an effort to determine maximum efficiency with the technique, we collected EDS data using a range of acquisition times (5, 10 and 30 second) to assess the effect of run time on results. In this sample, six mounds were analysed three times using 5, 10 and 30 second acquisition times. Thirdly, and again to maximize the technique's efficiency, we conducted analyses to investigate how to determine the minimum number of samples required to obtain results that represent the actual solute composition (s) of a fluid inclusion population. The number of analysis required to collected representative data is assessed by comparing results collected from samples for which we analyse 4, 8, 16 and 32 evaporate mounds.

SEM-EDS instrument calibration and synthesis of standards

To assess the performance of the EDS detector, we synthesized and analysed a series of salt standards. Standards are synthesized with salts composed of the major cation and anion species identified in mounds analysed during preliminary testing (i.e., mounds generated for evaluation of decrepitation temperature). To prepare synthetic salts, laboratory-standard NaCl and fluorite crystals were crushed and hand mortared to a very fine granular texture. Next, salt compounds were mixed to form a simple series of ratios that range from pure NaCl and pure fluoride salt (Table 2). Ideally, the matrix effects associated with these compounds chosen to make the synthetic mounds are similar to the matrix effects associated with evaporate mounds in SMB samples. In this study, F, Na, Cl, K and Ca are major solute species, and we corrected EDS data for F, Na, Cl and Ca using calibration curves constructed from the analysis of standards (Fig. 11).

Results

Petrography

Extent and degree of fluid–rock interaction in the South Mountain Batholith

To some extent, alteration assemblages occur in all SMB samples examined in this study. Petrographic observation of hundreds of SMB

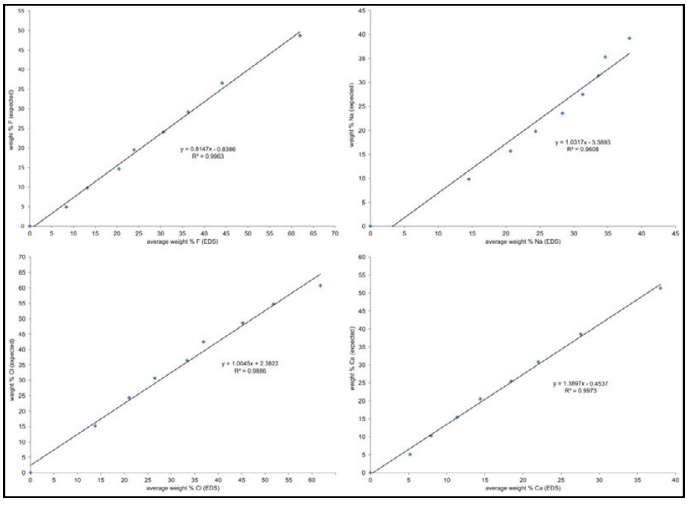

Figure 11 – Calibration curves for major cation and anion species in SMB mounds.

Table 2 – Composition of synthetic mounds. The compositional range of salt standards includes the expected compositional range of major solutes in evaporate mounds formed by decrepitation of fluid inclusions hosted in samples from study area.

Standard label	Mass (g)			Weight (mg)					Weight %				
	NaCl	CaF_2	Total	Na	Cl	Ca	F	Total	%Na	%Cl	%Ca	%F	Total
0	0.101	0.000	0.101	39.63	61.37	0.00	0.00	101.00	39.24	60.76	0.00	0.00	100.00
10	0.090	0.010	0.100	35.32	54.68	5.13	4.87	100.00	35.32	54.68	5.13	4.87	100.00
20	0.080	0.020	0.100	31.39	48.61	10.27	9.73	100.00	31.39	48.61	10.27	9.73	100.00
30	0.070	0.030	0.100	27.47	42.53	15.40	14.60	100.00	27.47	42.53	15.40	14.60	100.00
40	0.060	0.040	0.100	23.55	36.45	20.53	19.47	100.00	23.55	36.45	20.53	19.47	100.00
50	0.051	0.050	0.101	20.01	30.99	25.67	24.33	101.00	19.82	30.68	25.41	24.09	100.00
60	0.040	0.060	0.100	15.70	24.30	30.80	29.20	100.00	15.70	24.30	30.80	29.20	100.00
75	0.025	0.075	0.100	9.81	15.19	38.50	36.50	100.00	9.81	15.19	38.50	36.50	100.00
100	0.000	0.101	0.101	0.00	0.00	51.85	49.15	101.00	0.00	0.00	51.33	48.67	100.00

thin sections, it is known that alteration in SMB granitoids ranges from essentially unaltered samples (Fig. 12) to pervasively altered samples (Fig. 13). However, location data for samples in the western half of the batholith is not preserved, so mapping of petrographic data is limited to the eastern half of the batholith (Fig. 14). Several general patterns emerge from this data. Firstly, fluid inclusions occur in abundance throughout the batholith. Secondly, perthitic feldspar is much more abundant as patch perthite as compared to film and flame perthite. Thirdly, saussuritization, or the replacement of plagioclase by epidote occurs in much lower abundance than sericite (replacement of feldspar by clay minerals.

Evaporate Mound Analysis

Decrepitation temperature

The number of mounds generated during three oven heating runs at 325°C, 400°C and 500°C suggests a 500°C decrepitation temperature is preferable for mound generation. Within the experimental temperature range, mound size is largest in samples heated to 500°C and smallest in samples heated to 325°C (Fig. 15A) Further, results demonstrate that decrepitation temperature does not impact composition of evaporate mounds (Fig. 15B). The shape (i.e., morphology) and chemical diversity of mounds generated through the oven-decrepitation of SMB samples is displayed in Fig.16.

Oven versus stage heating and acquisition time

Decrepitation of chips from two samples (A09-2378 and A09-2370), using both oven and stage heating, produced Na-K rich mounds (Fig. 17). The median concentrations of Na, Cl and K in mounds generated by both methods in sample A09-2370 are comparable. However, the median concentration of Na, Cl and K in mounds in sample A09-2378 are consistently higher in stage-generated mounds.

Two important results emerge from the preliminary assessment of EDS analysis collected using 5, 10 and 30 second acquisition times. Firstly, the number of major solute species detected increases with acquisition time. The EDS signals for 5 second acquisition time includes four major solute species (F, Na, Cl and Ca), whereas 10 and 30 second acquisition times detected five major solute species (F, Na,

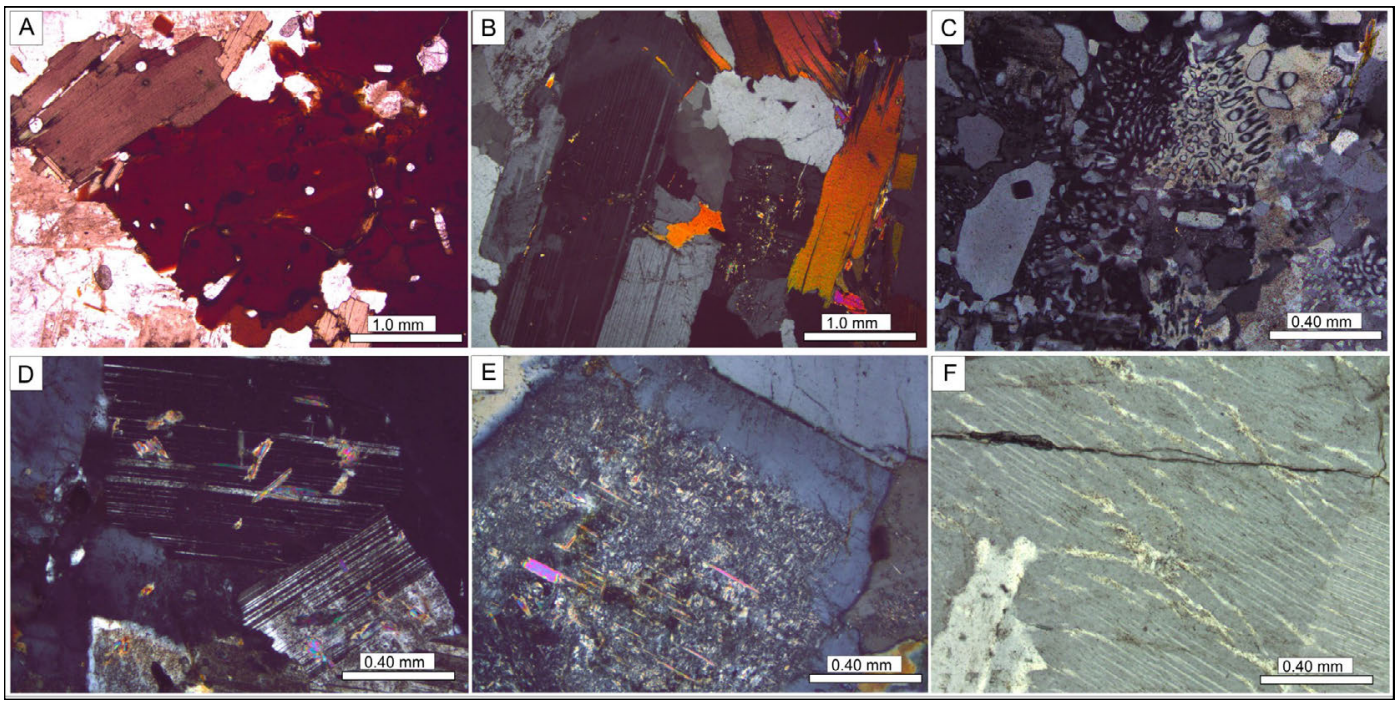

Figure 12 – Photomicrograph images of textures in unaltered SMB granitoids. (A) Sample D13-2-8-10: glomeroporphyritic texture defined by fresh reddish-brown biotite grains displaying numerous apatite inclusions. (B) Sample D13-2004: hypidomorphic granodiorite displaying coarse-grained (>0.5 mm), euhedral, tabular, zoned plagioclase phenocryst with incipient sericitization. (C) Sample D12-0121-1-C: pervasive graphic texture defined by blebby intergrowths of quartz and feldspar of inequigranular leucogranite consisting of fine- to medium-grained matrix minerals and coarse-grained unaltered quartz. (D) Sample A09-2095: incipient saussuritization and partial sericitization in euhedral plagioclase in holocrystalline granodiorite. (E) Sample D12-3074: seritization of zoned euhedral plagioclase displaying incipient muscovite development along cleavage planes. Note fluid inclusion trails hosted in along fracture planes in adjacent coarse-grained quartz. (F) Sample D05-0015: orthoclase megacryst displaying film and flame perthite.

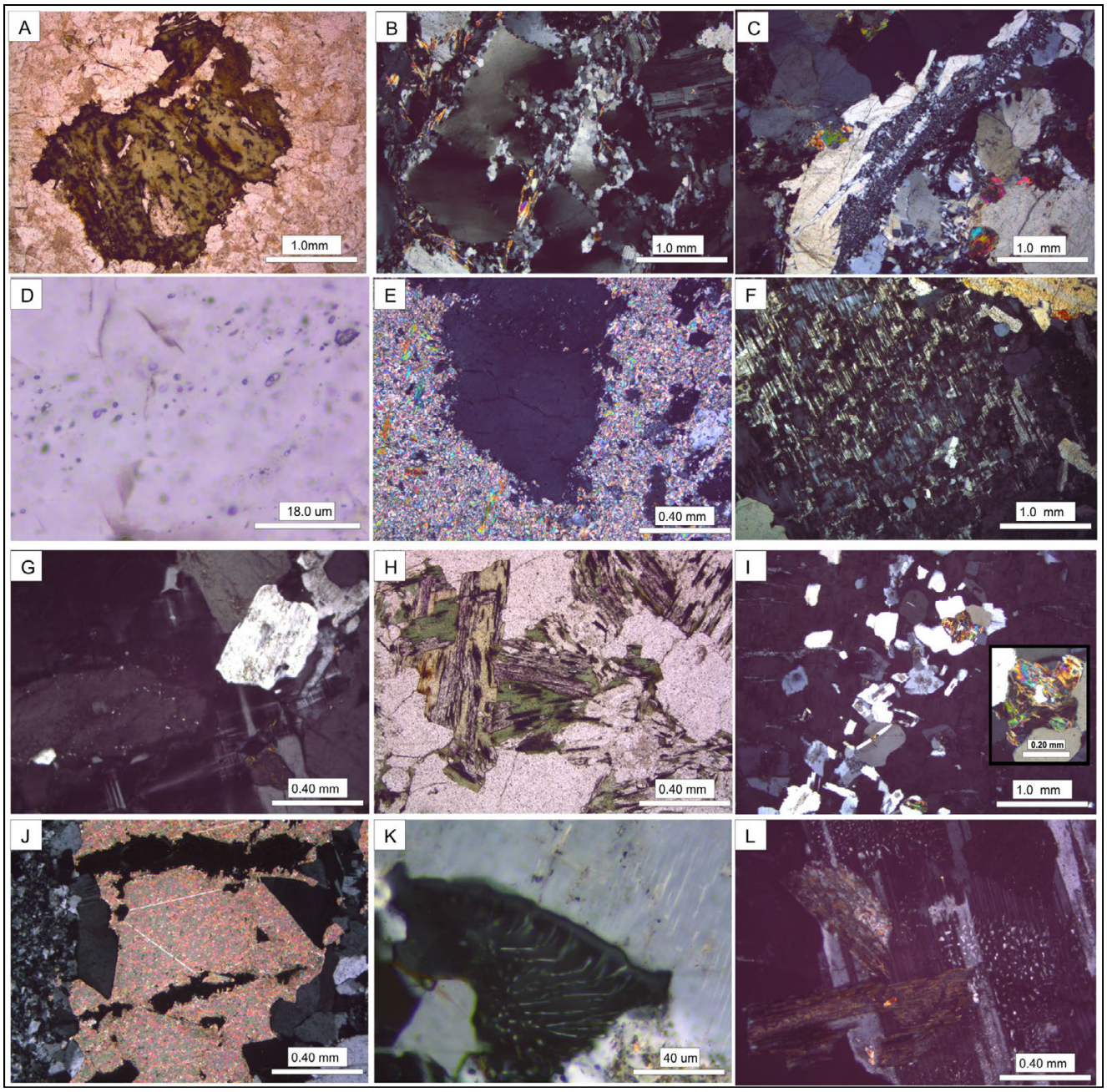

Figure 13 – Photomicrographs of thin sections of pervasively altered SMB granitoid samples. (A) Sample D13-2065. Extreme chloritization of biotite with abundant fine-grained opaque inclusions. Note sericitization of adjacent feldspar. (B) Sample A04-1054: Porphyritic granitoid displaying coarse-grained quartz phenocrysts with undulose texture and medium-grained plagioclase phenocrysts displaying kinked polysynthetic twin planes. Interstitial space filled with secondary fine-quartz grains and white mica. (C) Sample A09-2141: Fine-grained quartz grain filling fracture between quartz and feldspar phenocrysts. Quartz grain clearly inundated with fluid inclusions and graphic textures matrix displays pockets of white mica. (D) Sample A09-2141: high magnification photomicrograph of quartz-hosted fluid inclusions in hydrothermally altered granite. Inclusions are predominately 2-phase types with a liquid/vapour ratio of 95/5. (E) Extreme hydrothermal alteration texture. Primary feldspar components are hydrothermally altered, which results in crystallisation of fine-grained epidote and white mica. (F) Corse-grained perthitic feldspar displaying patchy albite and orthoclase. (G) Microcline domains adjacent to adjacent to subhedral quartz and feldspar grains in hypidomorphic granitoid. (H) Sample D12-0113-2: Chloritization of biotite glomerocryst and inundation of fluid inclusions through all mineral phases evidenced by dusty texture. (I) Sample D12-3071: Coarse-grained poikilitic feldspar with blebby quartz inclusions and sparse pinitized cordierite (inset). (J) Euhedral fluorite (isometric) grains ingrown with calcite (high relief) in pervasively altered granitoid. (K) Sample D12-0039. Myrmekitic texture with fine-grained vermicular quartz included in plagioclase adjacent to alkali feldspar. Note flame perthite in feldspar. (L) Sample D12-0113-1. Myrmekitic texture in albitic plagioclase defined by vermicular intergrowths of quartz. Note also the chloritized biotite intergrown into the plagioclase.

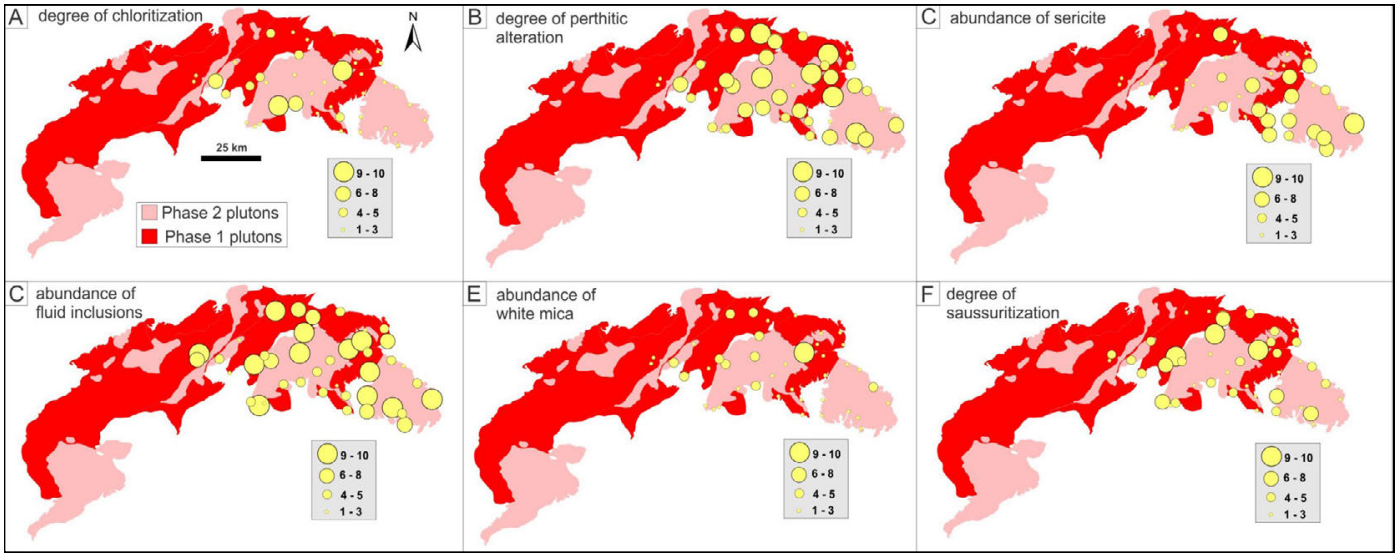

Figure 14 – Proportional symbol plot showing distributions of hydrothermal alteration textures in SMB granitoids. (A-F) Proportional circle sizes represent the degree of alteration assemblages and the abundance of sericite, white mica and fluid inclusions. Scales are qualitative (no units) and grouped into three categories: minimal alteration (1-4), moderate (5-7) and pervasive (8-10).

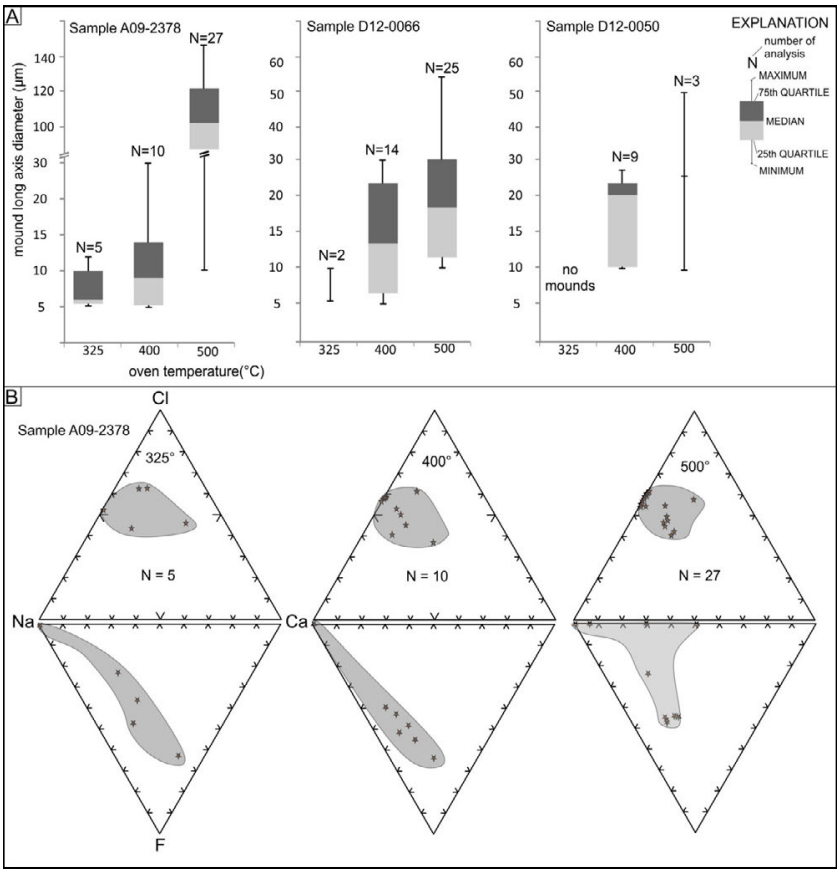

Figure 15 – (A) Box and whisker plots of observable mound size versus decrepitation temperature. The important observation is that the mounds generated by heating quartz grains to 500°C are larger and more abundant than mounds generated at 325°C and 400°C. (B) Ternary plots of major cation species concentration (normalised wt%) in mounds generated by heating to 325°C, 400°C and 500°C. The important point is that mound composition is unaffected by decrepitation temperature.

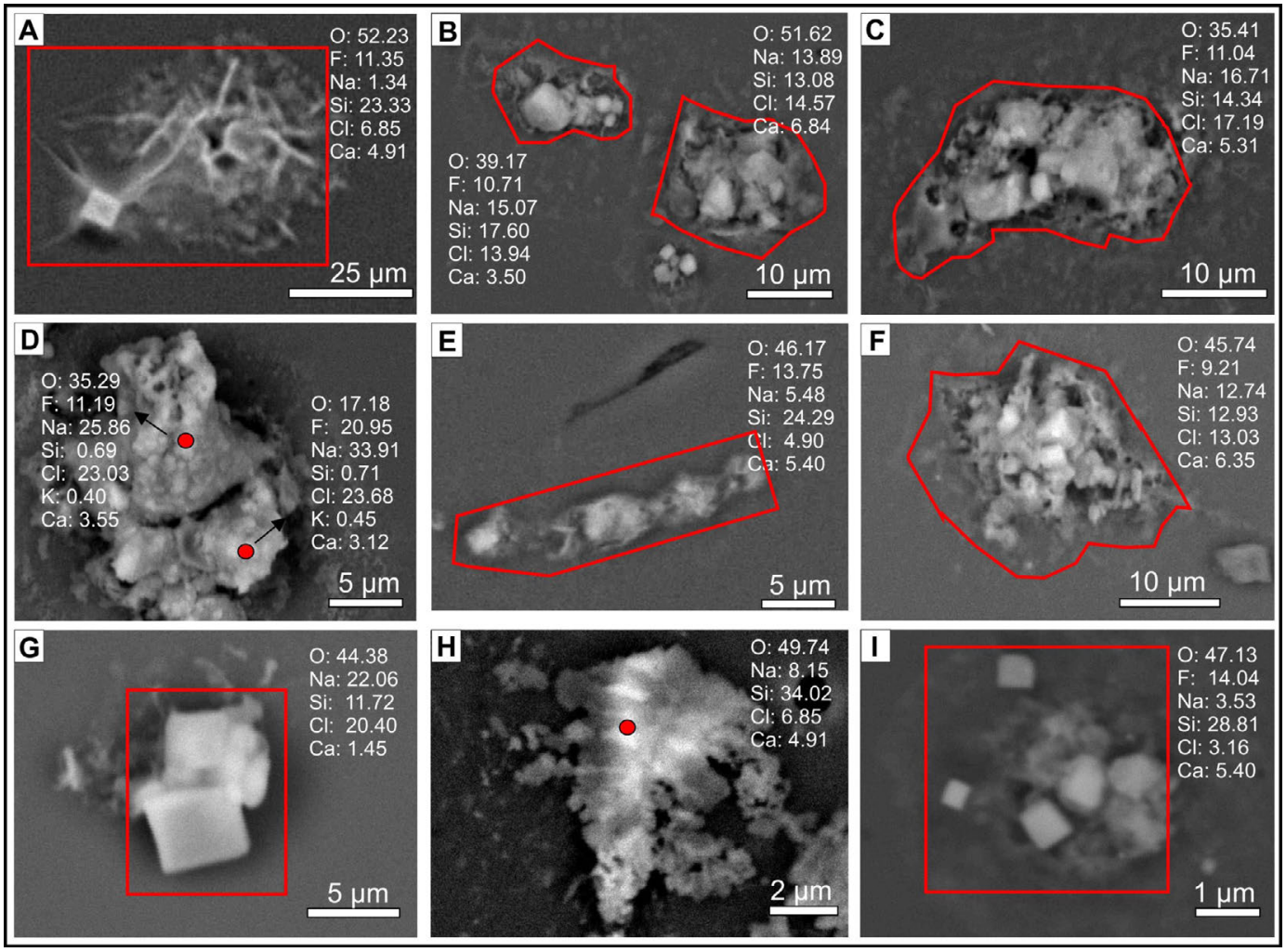

Figure 16 – Evaporate mounds generated through decrepitation (500°C) of SMB fluid inclusions hosted by quartz. (A – I) Chemical composition of mounds analysed in raster mode (outlined by red boxes) or point mode (red dots). Units for chemical composition are atomic concentrations in mound (normalised to 100%).

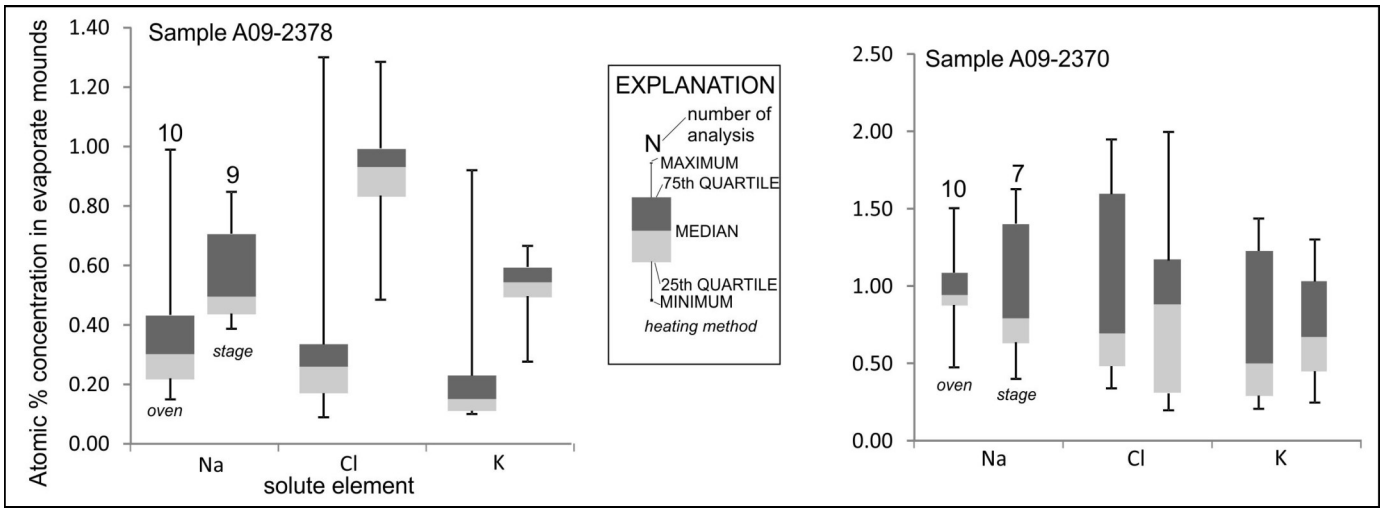

Figure 17 – Box plots comparing results from EDS analysis of oven- and stage-heated samples. The number of Na-Cl-K mounds generated by these methods is comparable, suggesting that heating rate does not have an effect on mound generation.

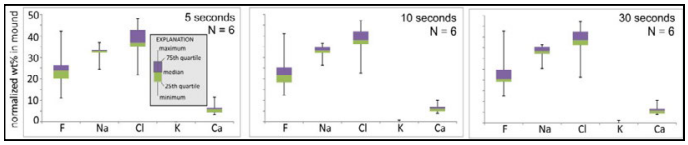

Figure 18 – Box plots of major solute concentration versus EDS acquisition time. Concentrations of major solute species in mounds EDS data generated using 5, 10 and 30 second run times are consistent.

Cl, K and Ca). Secondly, the concentrations of major solute species in the results for 5, 10 and 30 second acquisition times are consistent (Fig.18).

Calibration for major solute species

An assessment of default-calibrated data and custom-calibrated data are shown in Fig. 19. Comparing the two data sets reveals a distinct trend: default EDS settings result in an over-reporting of fluorine and sodium, and an under-reporting for chlorine and calcium. The discrepancy between default- and custom-calibrated data is greatest in F and Ca.

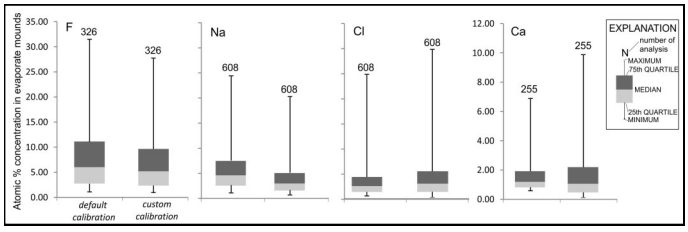

Figure 19 – Box plots of element concentration in evaporate mounds for major solutes in SMB quartz-hosted fluid inclusions. The EDS analyser used in this research, a correction needed to be applied due to an overestimation of F and Na and an under estimation for Cl and Ca.

Number of analyses

From the assessment of results obtained from two samples in which 4, 8, 16 and 32 mounds were analysed, there is consistent number of major solute species detected. The concentration range of major solute species however does vary with number of analysis. However, this variation shows no consistent pattern in F, Na and Cl. However, the median values and range in Ca concentrations appears to be less variable than other major solute species (Fig. 20).

Raster vs. point analysis

Two important points emerge from assessing EDS data obtained from raster- and point-mode analysis of evaporate mounds. Firstly, both point-mode analyses substantiate mound heterogeneity (Fig. 21) Point analysis reveals that the solute composition of mounds is not uniform as elements tend to concentrate in discrete domains within the mound. Secondly, point mode analysis reveals elements that are not detectable in raster analysis (Fig. 22). Although multiple point analyses can provide average compositions for major solute species that are comparable to raster analysis results (Fig 22), minor solute components (e.g., S) may not be detected. In addition, X-ray maps reveal that sodium chloride and calcium fluoride salts are the dominant salt compounds in SMB decrepitate mounds (Fig. 23).

Identifying different fluids

Following screening of the initial data set for internal consistency, 517 good mound analyses were retained for further analysis. Of these, 133 are from Phase 1 samples (n = 20) and 384 are from Phase 2 samples (n = 46). The chemical composition of Phase 1 pluton fluid inclusions is clearly dominated by F-Na-Cl-Ca fluid. In addition, Phase 1 pluton samples host fluid inclusions that contain trace concentrations of S, Zn, Fe, Mo and V (Fig 24A). Conversely, the chemical composition of Phase 2 pluton fluid inclusions include two populations: a Na-K fluid and a F-Na-Cl-Ca fluid. Phase 2 pluton hosted fluid inclusions carry trace concentrations of S, F, Mo, Mn, Sn and Yb (Fig. 24B).

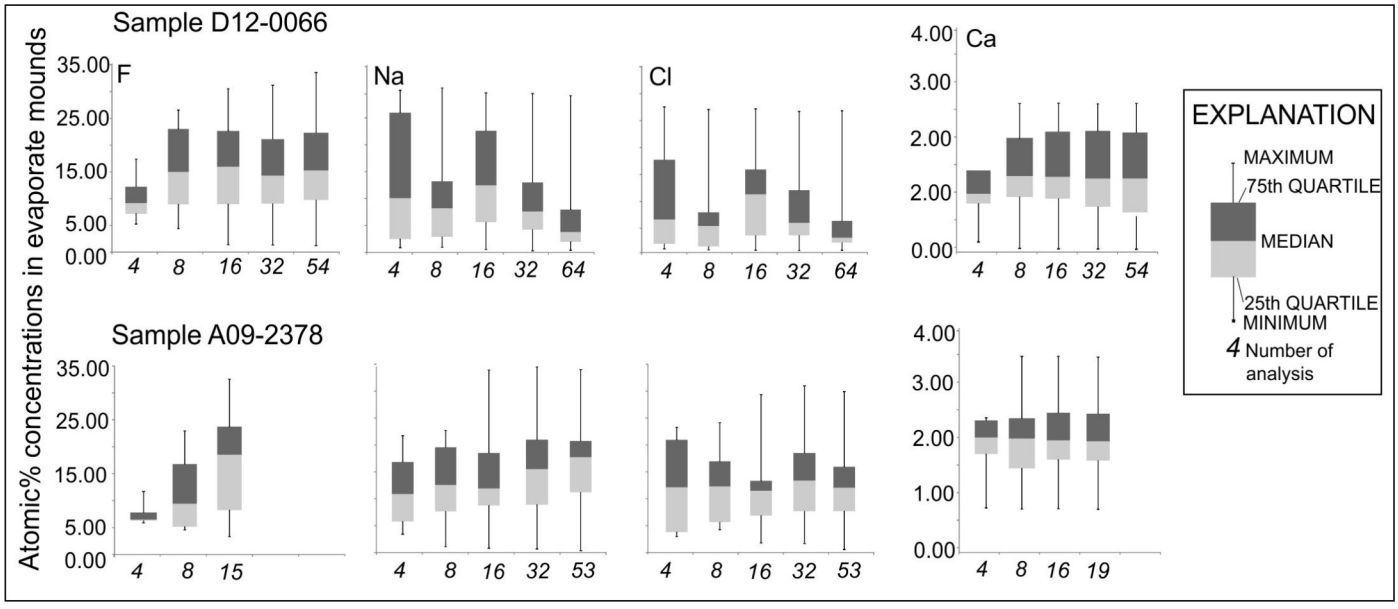

Figure 20 – Box plots of major element concentrations in mounds verses number of analysis.

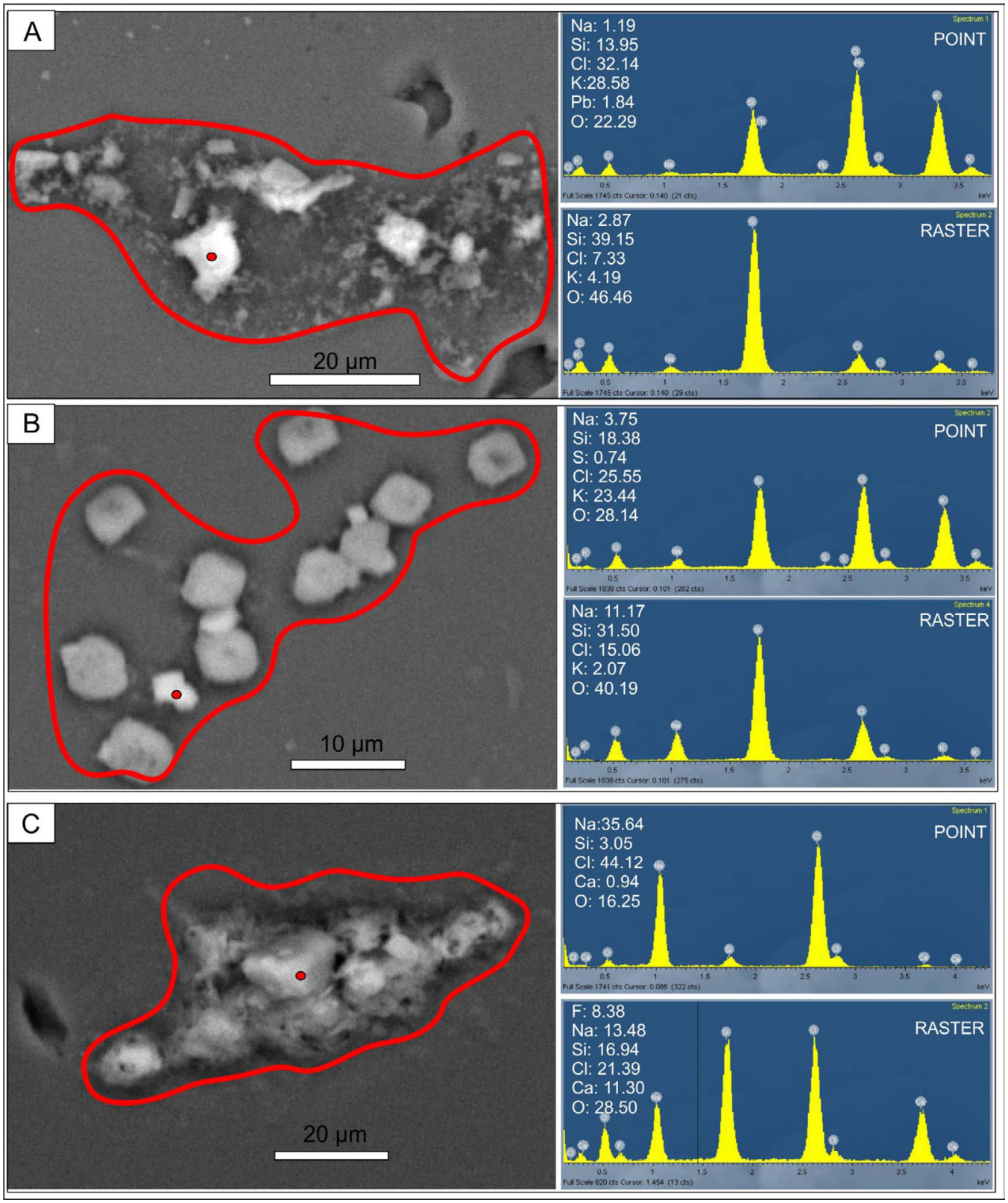

Figure 21 – Backscattered electron (BSE) images of evaporate mounds and corresponding EDS signals. (A) Na-Cl-K rich mound piled next to empty vugs (i.e., evacuated fluid inclusion pit). Point analysis histogram also reveals presence of lead decrepitate. (B) Cubic-shaped Na-Cl rich evaporate mounds. Point analysis reveals presence of sulphur residue. (C) F-Na-Cl-Ca rich evaporate mound. Note that presence of F and Ca is not resolved in point analysis. Elemental abundance for solute species in mounds in atomic concentrations.

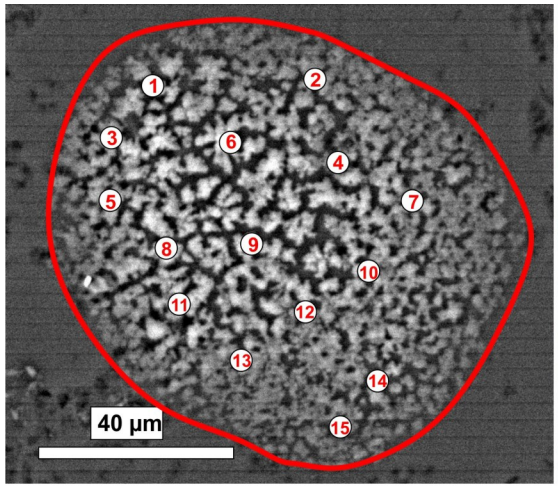

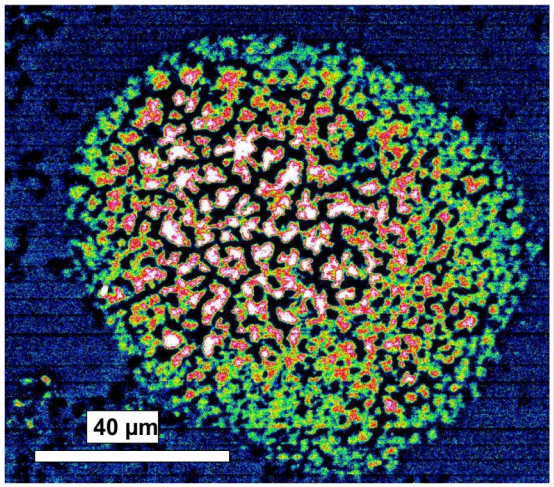

Point	O	Na	Si	Cl	K	Ca
1	66.08	2.85	29.71	1.21	0.15	
2	60.69	6.48	27.20	4.49	1.14	
3	46.95	14.88	29.05	8.83	0.30	
4	58.62	6.53	31.24	3.61		
5	53.08	6.70	33.31	5.33	1.59	
6	47.81	14.74	26.83	9.93	0.70	
7	50.40	16.08	23.76	8.92	0.63	0.21
8	58.59	4.80	34.17	2.44		
9	48.79	11.82	32.22	6.86	0.32	
10	43.92	13.65	34.07	7.83	0.53	
11	41.25	15.18	33.31	9.82	0.44	
12	47.13	15.81	27.34	9.00	0.54	0.18
13	56.65	10.32	27.46	5.57		
14	51.46	16.90	22.16	9.14	0.35	
15	53.50	10.86	28.93	6.41	0.30	
Average	52.33	11.17	29.38	6.63	0.47	0.03
Raster	53.19	11.73	28.61	6.10	0.38	

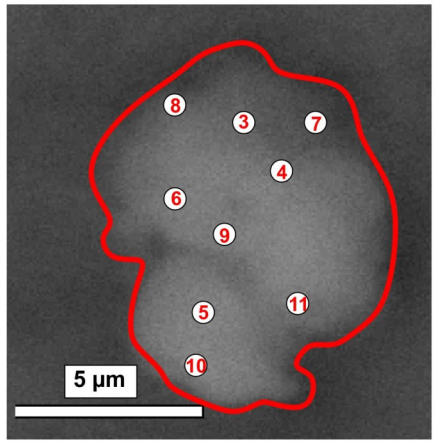

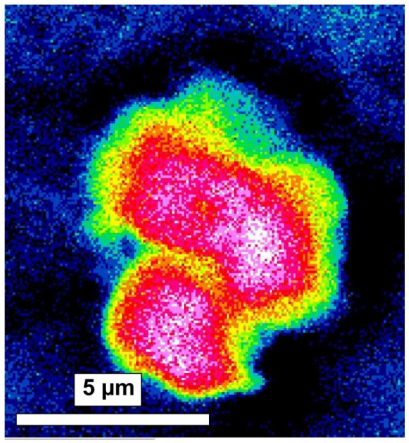

Point	O	F	Na	Al	Si	S	Cl	K	Ca	Cu	Pb
3	30.99	19.01	20.15		13.02	0.09	14.47		2.27		
4	29.51	17.00	25.32	0.15	9.31		16.45		2.26		
5	40.28	10.50	23.35		10.22	0.06	14.48	0.05	1.06		
6	27.07	14.76	27.39		10.94		18.35		1.49		
7	40.08	14.25	10.57		22.19		10.23		2.51	0.16	
8	38.23	19.69	14.42		16.31	0.13	9.36		1.86		
9	32.77	20.68	20.38		12.09	0.13	12.03		1.93		
10	39.21	16.62	16.45		9.57		7.98		1.06		
11	40.47	11.42	14.14		20.18		11.51		2.20		0.07
Average	35.40	15.99	19.13	0.02	13.76	0.05	12.76	0.01	1.85	0.02	0.01
Raster	36.79	15.96	19.38		13.92		12.32		1.64		

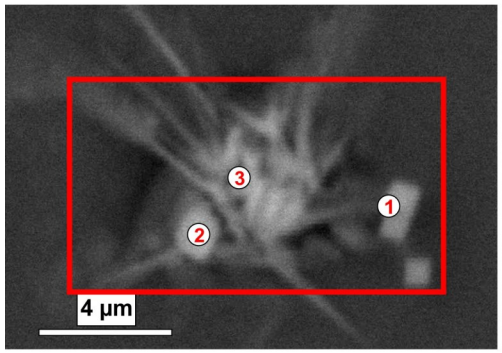

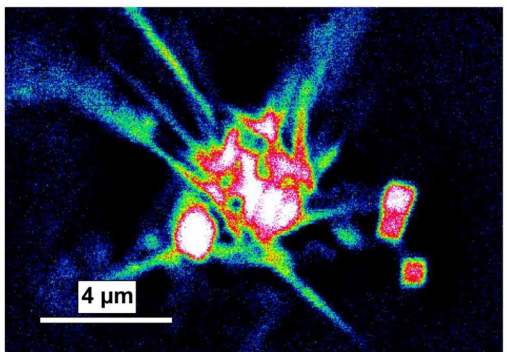

Point	O	F	Na	Si	S	Cl	Ca
1	52.21	7.53	9.3	23.86	0	5.87	1.23
2	22.73	16.24	16.38	26.94	0.41	13.21	4.08
3	30.61	23.61	8.58	24.78	0	7.24	5.18
Average	35.18	15.79	11.42	25.19	0.14	8.77	3.50
Raster	40.04	21.06	2.63	30.29		2.28	3.7

Figures 22 – Backscattered electron (BSE) images (grey scale and false-colour scale) of evaporate mounds and corresponding EDS data. Note that heavier (i.e., metallic) solutes are readily imaged using this technique, and EDS point mode provides better resolution of minor solute components compared to raster mode. Mound compositions and point analyses given in atomic concentrations.

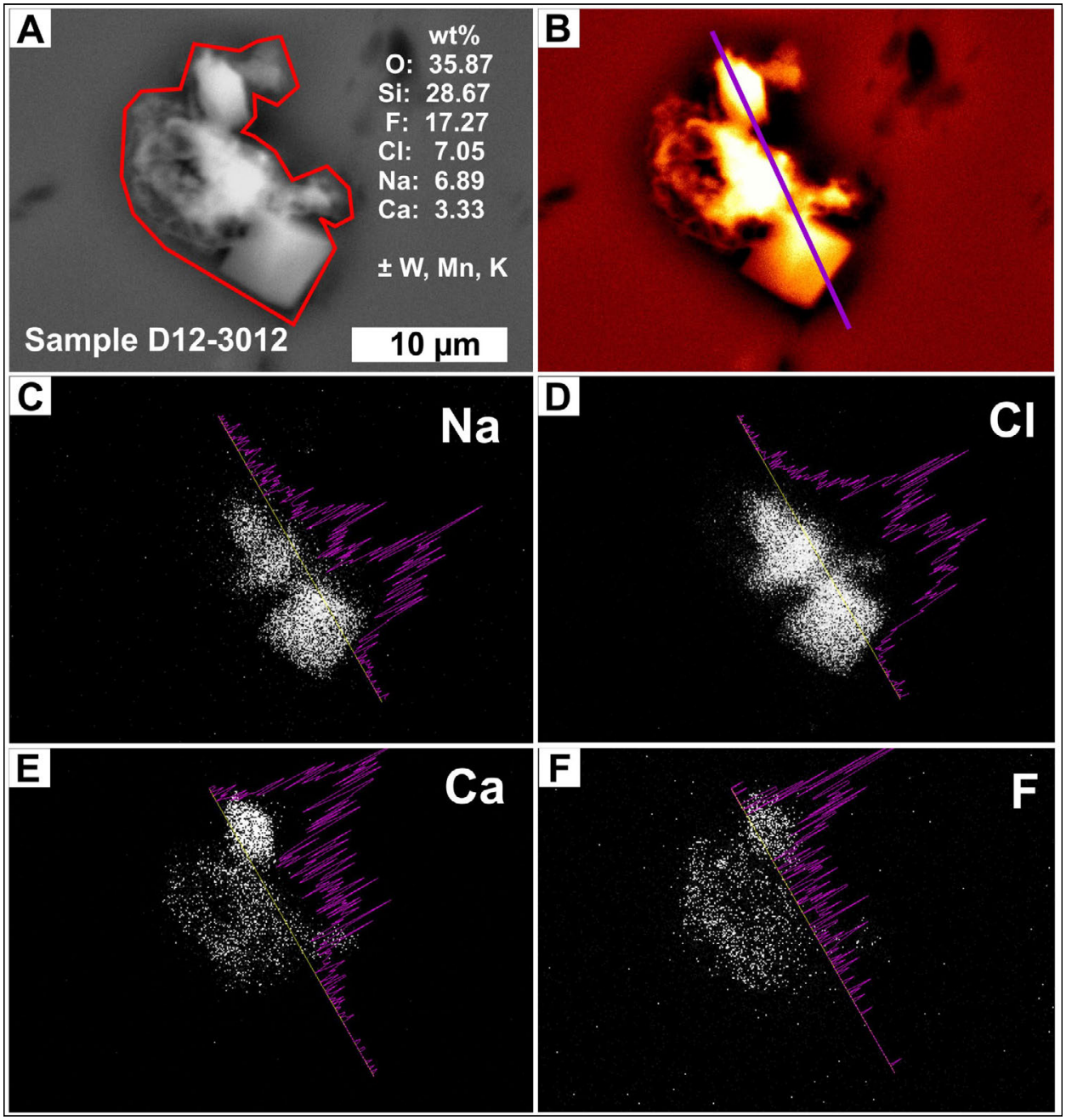

Figure 23 – BSE image and X-ray map analysis of evaporate mound. (A) BSE image of evaporate mound showing raster area in red outline. (B) False-colour BSE image of evaporate mound showing X-ray transect. (C-D) X-ray maps of sodium and chlorine. Light-coloured (i.e., bright) areas correspond to areas of high concentration of corresponding element. (E-F) X-ray maps of calcium and fluorine. These images show the chemical composition of salt compounds that compose evaporate mounds.

Discussion

In-situ fluid inclusion composition analysis

All magmatic-hydrothermal mineral deposits share a common history, which includes magma fractionation, evolution of an aqueous, multi-component fluid phase, partitioning of the fluid phase, fluid migration into new T-P-X environments, and eventual precipitations of metals. Evaluating the chemistry of magmatic-hydrothermal fluids is useful for understanding mineral crystallisation if the bulk solute composition of the mineralizing fluid(s) is accurately determined. Evaporate mound analysis is a unique analytical technique because it permits in-situ solute characterization of the mineralizing fluids preserved as fluid inclusions in rock-forming minerals. Furthermore, this method resolves the presence of different fluids within single coarse-grained quartz by analysing solutes in evaporate mounds formed during the decrepitation of variable-sized (i.e., 1 to >30 µm long-axis diameters) fluid inclusions in a cost-effective and time efficient manner.

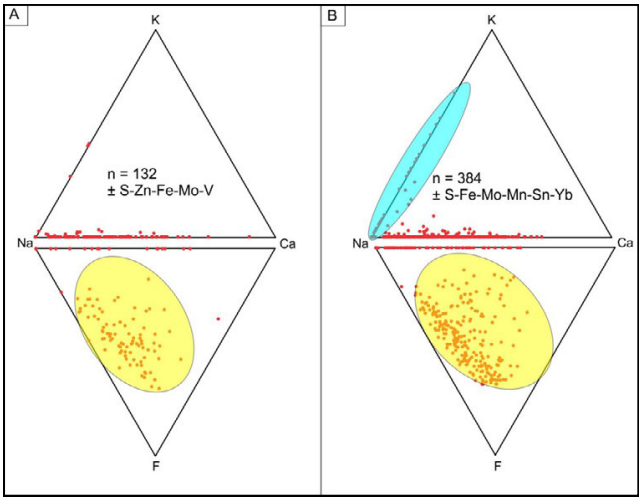

Figure 24 – Ternary plots of SMB fluid inclusion solute compositions. (A) Phase 1 fluid inclusions compositional data. A fluid inclusion population consisting of F-Na-Cl-Ca highlighted. (B) Phase 2 fluid inclusion compositional data. Two fluid inclusion populations highlighted: one consisting of Na-K and another consisting of F-Na-Cl-Ca.

Significance of resolving fluid compositions

The SEM-EDS methodology described herein resolves the solute composition of fluid inclusions using simple and effective analytical procedures. The results produced from the analysis of SMB quartz-hosted fluid inclusions in this study provide average solute compositions for a large number (n = 66) of samples. These data record the presence of elevated Ca, including those from the chemically evolved, therefore calcium-depleted, rocks, and the pervasive occurrence of fluorine in samples that are distal to any known mineralisation. The Ca-bearing fluid may be considered to reflect the petrographic observation of extensive albitization of plagioclase, which occurs in all samples. This alteration process could involve a coupled dissolution-precipitation reaction (which leaves a distinctive pitted texture in the altered the feldspar and liberated calcium to the fluid (Putnis, 2002). The process is attributed to the reaction of an orthomagmatic fluid with already crystallised granite, although it does not preclude some Ca contribution from a wall-rock metamorphic fluid, as indicated from stable isotopes (Kontak and Kyser, 2011).

Another point worthy of further discussion is the unexpected enrichment of F in the fluid inclusion F-Na-Ca population, which is likely the first recognition of this phenomenon in granitic bodies on such a scale anywhere. The pervasive occurrence of F in the sample set suggests that the generation of this F-rich fluid is part of the natural evolution of the system and consistent with the presence of topaz in the most evolved magmatic rocks and as part of mineralised greisens. Finally, that F enrichment occurs in the same fluid with Ca indicates a possible cause and effect relationship which we suggest relates to the reactive capacity of the original exsolved Na-F fluid.

Future studies

Outstanding questions about the technique should guide the direction of future work. Firstly, in order to relate alteration assemblages to fluid-inclusion compositions, petrographic work on samples for which we have mound data must be completed. Secondly, more work is required to explain the variation in data between oven-generated mounds and stage-generated mounds. Thirdly, we have grouped samples by pluton, which is the broadest rock classification identified in the SMB. NSDNR mapping identifies 260 mappable SMB rock units, which is an available mapping guide for future evaporate mound analysis work.

The usefulness of the technique as an exploration tool for vectoring towards areas of mineralisation is not yet known. Application of evaporate mound analysis to a local-scale study area (i.e., 1 or 2 km^2 area) would provide an opportunity to assess how the technique may be useful to industry.

Acknowledgments

This fluid inclusion study was supported by the Canadian Federal Government's Research Affiliate Program and contributes towards the fulfilment of objectives for the Targeted Geoscience Initiative 4. This component of the project also represents the academic and professional research that can be generated by formal cooperation between the Geological Survey of Canada and Saint Mary's University Department of Geology. This work provides an example of the complementarity between these two institutions. Well-beyond formal commitments, this project owes its success and to the dedicated initiatives of Dr Jacob Hanley (Saint Mary's University, Halifax), Dr Dan Kontak (Laurentian University, Sudbury) and Dr Neil Rogers (Geological Survey of Canada, Ottawa). A summary of the raw data generated by the study is presented in this report, and the complete data set is available to anyone who may wish to view it, and is available from the Magmatic Ore Deposits Laboratory, Department of Geology, Saint Mary's University, 923 Robie Street, Halifax, Nova Scotia.

The first author would like to express his many thanks to Drs Jacob Hanley and Daniel Kontak for conceiving this project and giving freely of their time in assisting with the design and execution of this project. And a great deal of thanks is owed to Dr Neil Rogers for guidance during field work in Yarmouth County and the New Ross area, as well as help with various reports produced throughout the past two years. Tracy Lenfesty, Dr Chris White, Dr Bob Ryan and Mick O'Neill are acknowledged for providing access to samples at the Nova Scotia Department of Natural Resources (NSDNR).

References

Anderson, A.J., and Mayanovic, R.A., 2003. Electron, nuclear and X-ray probe microanalysis of fluid inclusions; *in* Fluid Inclusions: Analysis and Interpretation, (ed.) I. Samson, A.J. Anderson and D. Marshall; Mineralogical Association of Canada Short Course Publication, p. 323-352.

Bu, X., Wang, T., and Hall, G., 2003. Determination of halogens in organic compounds by high resolution inductively coupled mass spectrometry; Journal of Analytical Atomic Spectrometry, v. 18, p. 1443-1451.

Carruzzo, S., Kontak, D.J., and Clarke, D.B., 2000. Granite-hosted mineral deposits of the New Ross area, South Mountain Batholith, Nova Scotia, Canada: Constraints of fluids using fluid inclusion thermometry and decrepitate analysis; Transactions of the Royal Society of Edinburgh: Earth Sciences, v. 91, p. 303-319.

Chatterjee, A.K., and Clarke, D.B., 1985. Physical and chemical processes in the South Mountain Batholith; *in* Recent Advances in the Geology of Granite-Related Mineral Deposits, Proceed-

ings of the CIM Conference on Granite-Related Mineral Deposits, (ed.) R.P. Taylor and D.F. Strong; The Canadian Institute of Mining and Metallurgy: Special volume 39, p. 223-233.

Chi, G., Chou, I.M., and Lu, H., 2003. An overview on current fluid-inclusion research and applications; Acta Petrologica Sinica, v. 19, p. 201-212.

Chryssoulis, S., and Wilkinson, N., 1983. High silver content of fluid inclusions in quartz from Guadalcazar Granite, San Luis Potosi, Mexico: A contribution to ore-genesis theory; Economic Geology, v. 78, p. 302-318.

Clarke, D.B., and Halliday, A.N., 1980. Strontium isotope geology of the South Mountain Batholith, Nova Scotia; Geochimica et Cosmochimica Acta, v. 44, p. 1045-1058.

Clarke, D.B., MacDonald, M.A., Reynolds, P.H., and Longstaffe, F.J., 1993. Leucogranites from the eastern part of the South Mountain Batholith, Nova Scotia; Journal of Petrology v. 34, p. 653-679.

Corey, M.C., 1994. Diamond-drilling of rare element pegmatites in southwestern Nova Scotia; *in* Mines and Minerals Branch, Report of Activities 1993, (ed.) D.R. MacDonald; Nova Scotia Department of Natural Resources, Report 94-01, p. 65-79.

Corey, M.C., and Horne, R.J., 1989. Polymetallic-precious metal potential of the Tobeatic fault zone in southwestern Nova Scotia; Nova Scotia Department of Mines and Energy Report 89-1, p. 27-36.

Cormier, C.F.M., 1988. Greisenization and metasomatism associated with the Meguma – South Mountain Batholith contacts, Inglisville, Nova Scotia; unpublished BSc thesis, Saint Francis Xavier University, Antigonish, Nova Scotia, 81 p.

Diamond, L.W., Marshall, D.D., Jackman, J.A., and Skippen, G.B., 1990. Elemental analysis of individual fluid inclusions in minerals by Secondary Ion Mass Spectrometry (SIMS): Application to cation ratios of fluid inclusions in an Archaean mesothermal gold-quartz vein; Geochimica et Cosmochimica Acta, v. 54, p. 545-552.

Frantz, J.D., Mao, H.K., Zhang, Y-G., Wu, Y., Thompson, A.C., Underwood, J.H., Giauque, R.D., Jones, K.W., and Rivers, M.L., 1988. Analysis of fluid inclusions by X-ray fluorescence using synchrotron radiation; Chemical Geology, v. 69, p. 235-244.

Giles, P.S., 1985. A major post-Visean sinistral shear zone – New perspectives on Devonian and Carboniferous rocks of Southern Nova Scotia; *in* Guide to Granites and Mineral Deposits of Southwestern Nova Scotia, (ed.) A.K. Chatterjee and D.B. Clarke; Nova Scotia Department of Mines and Energy, paper 85-3, p. 233-248.

Gleeson, S., 2003. Bulk analysis of volatiles in fluid inclusions; *in* Fluid Inclusions: Analysis and Interpretation, (ed.) I. Samson, A.J. Anderson and D. Marshall; Mineralogical Association of Canada Short Course Publication, p. 247-278.

Halter, W.F., Williams-Jones, A.E., and Kontak, D.J., 1996. The role of greisenization in cassiterite precipitation at the East Kemptville Tin Deposit, Nova Scotia; Economic Geology, v. 91, p. 368-385.

Haynes, F.M., and Kesler, S.E., 1987. Chemical evolution of brines during Mississippi Valley-type mineralization: evidence from East Tennessee and Pine Point; Economic Geology, v. 82, p. 53-71.

Haynes, F.M., Sterner, S.M., and Bodnar, R.J., 1988. Synthetic fluid inclusions in natural quartz. IV. Chemical analyses of fluid inclusions by SEM/EDA: Evaluation of method; Geochimica et Cosmochimica Acta, v. 52, p. 969-977.

Heinrich, C.A., and Cousens, D.R., 1989. Semi-quantitative electron microprobe analysis of fluid inclusion salts from the Mount Isa copper deposit (Queensland, Australia); Geochimica et Cosmochimica Acta, v. 53, p. 21-28.

Horne, R.J., MacDonald, M.A., Corey, M.C., and Ham, L.J., 1992. Structure and emplacement of the South Mountain Batholith, southwestern Nova Scotia; Atlantic Geology, v. 28, p. 29-50.

Kontak, D.J., 1990. The East Kemptville muscovite-topaz leucogranite. I. Geological setting and whole rock geochemistry; Canadian Mineralogist, v. 28, p. 787-825.

Kontak, D.J., 2004. Analysis of Evaporate mounds as a compliment to fluid-inclusion – thermometric data: case studies from granitic environments in Nova Scotia and Peru; Canadian Mineralogist, v. 42, p. 1315-1327.

Kontak, D.J., and Kyser, K., 2011. A fluid inclusion and isotopic study of an intrusion-related gold deposit (IRGD) setting in the 380 Ma South Mountain Batholith, Nova Scotia, Canada: evidence for multiple reservoirs; Mineralium Deposita, v. 46, p. 337-363.

Kontak, D.J., Ansdell, K., and Archibald, D., 1999. New constraints on the age and origin of the Dunbrack Pb-Cu-Zn-Ag deposit, Musquodoboit Batholith, southern Nova Scotia; Atlantic Geology, v. 35, p. 19-42.

MacDonald, M.A., 2001. Geology of the South Mountain Batholith, southwestern Nova Scotia; Nova Scotia Department of Natural Resources, Open File Report ME 2001-2, 281 p.

MacDonald, M.A., and O'Reilly, G.A., 1989. Gold enrichment associated with post-magmatic processes in the South Mountain batholith, southwestern Nova Scotia; Nova Scotia Department of mines and Energy Report 89-1, p. 13-25.

MacDonald, L.A., Barr, S.M., White, C.E., and Ketchum, J.W.F., 2002. Petrology, age, and tectonic setting of the White Rock Formation, Meguma terrane, Nova Scotia: evidence for Silurian continental rifting; Canadian Journal of Earth Sciences, v. 39, p. 259-277.

McPhie, J., Kamentsky, V., Allen, S., Ehrig, K., Agangi, A., and Bath, A., 2011. The fluorine link between a supergiant ore deposit and a silicic large igneous province; Geology, v. 39, p. 1003-1006.

Ménez, B., Phillippot, P., Bonnin-Mosbah, M., Simionovici, A., and Gibert, F., 2002. Analysis of individual fluid inclusions using synchrotron X-ray fluorescence microprobe: Progress toward calibration for trace elements; Geochimica et Cosmochimica Acta, v. 66, p. 561-576.

Muecke, G.K., and Clarke, D.B., 1981. Geochemical evolution of the South Mountain Batholith, Nova Scotia: Rare-Earth-Element evidence; Canadian Mineralogist, v. 19, p. 133-145.

O'Reilly, G.A., 1992. Petrographic and geochemical evidence for a hypogene origin of granite-hosted, vein-type Mn mineralization at the New Ross Mn deposits, Lunenburg County, Nova Scotia, Canada; Economic Geology, v. 87, p. 1275-1300.

O'Reilly, G.A., 2011. The Long Lake Mo-W-Cu greisens: A classic example of greisen development. Nova Scotia Department of Natural Resources Minerals Update Newsletter 28, p. 5.

O'Reilly, G.A., 2013. Granite- and metasediment-hosted W-Sn-Mo-Cu-Zn-Ag-Au at Westfield, Queens County; Nova Scotia Department of Natural Resources Minerals Update Newsletter 30, p. 4.

Putnis, A., 2002. Mineral replacement reaction: from macroscopic observations to microscopic mechanisms; Mineralogical Magazine, v. 66, p. 689-708.

Reynolds, P. H., Zentilli, M., and Muecke, G.K., 1981. K-Ar and $^{40}Ar/^{39}Ar$ geochronology of granitoid rocks from southern Nova Scotia: Its bearing on the geochemical evolution of the Meguma Zone of the Appalachians; Canadian Journal of Earth Sciences, v. 18, p. 386-394.

Roedder, E., and Bodnar, B., 1997. Fluid inclusion studies of hydrothermal ore deposits; *in* Geochemistry of Hydrothermal Ore Deposits, Third edition, (ed.) H.L. Barnes; p. 657-698.

Samson, I.M., Williams-Jones, A.E., and Lui, W., 1995. The chemistry of hydrothermal fluids in carbonitites: Evidence from leachate and SEM-decrepitate analysis of fluid inclusions from Oka, Quebec, Canada; Geochimica et Cosmochimica Acta, v. 59, p. 1979-1989.

Savard, M.M., and Chi, G., 1998. Cation study of fluid inclusion decrepitates in the Jubilee and Gays River (Canada) Zn-Pb deposits – characterization of ore-forming brines; Economic Geology, v. 93, p. 920-931.

Smith, T.E., and Turek, A., 1976. Tin-bearing potential of some Devonian granitic rocks in S.W. Nova Scotia; Mineralium Deposita, v. 11, p. 234-245.

Thomas, R., Webster, J.M., Rhede, R., Seifert, W., Rickers, K., Förster, H.J., Heinrich, R., and Davidson, P., 2006. The transition from peraluminous to peralkaline granitic melts: Evidence from melt inclusions and accessory minerals; Lithos, v. 91, p. 137-149.

Timofeeff, M.N., Lowenstein, T.K., and Blackburn, W.H., 2000. ESEM-EDS: an improved technique for major element chemical analysis of fluid inclusions; Chemical Geology, v. 164, p. 171-182.

Walsh, J.F., Kesler, S.E., Duff, D., and Cloke, P.L., 1988. Fluid inclusion geochemistry of high-grade, vein-hosted gold ore at Pamour Mine; Porcupine Camp, Ontario; Economic Geology, v. 83, p. 1347-1367.

Wilkinson, J.J., 2001. Fluid inclusions in hydrothermal ore deposits; Lithos, v. 55, p. 229-272.

Williams-Jones, A.E., Samson, I.M., and Olivo, G.R., 2000. The genesis of hydrothermal fluorite-REE deposits in the Gallinas Mountains, New Mexico; Economic Geology, v. 95, p. 327-342.

Zaw, K., Hunns, S.R., Large, R.R., Gemmell, J.B., Ryan, C.G., and Mernagh, T.P., 2003. Microthermometry and chemical composition of fluid inclusions from the Mt Chalmers volcanic-hosted massive sulphide deposits, central Queensland, Australia: implications for ore genesis; Chemical Geology, v. 194, p. 225-244.